Thermal-emission

Geometry and color of the different ejecta components

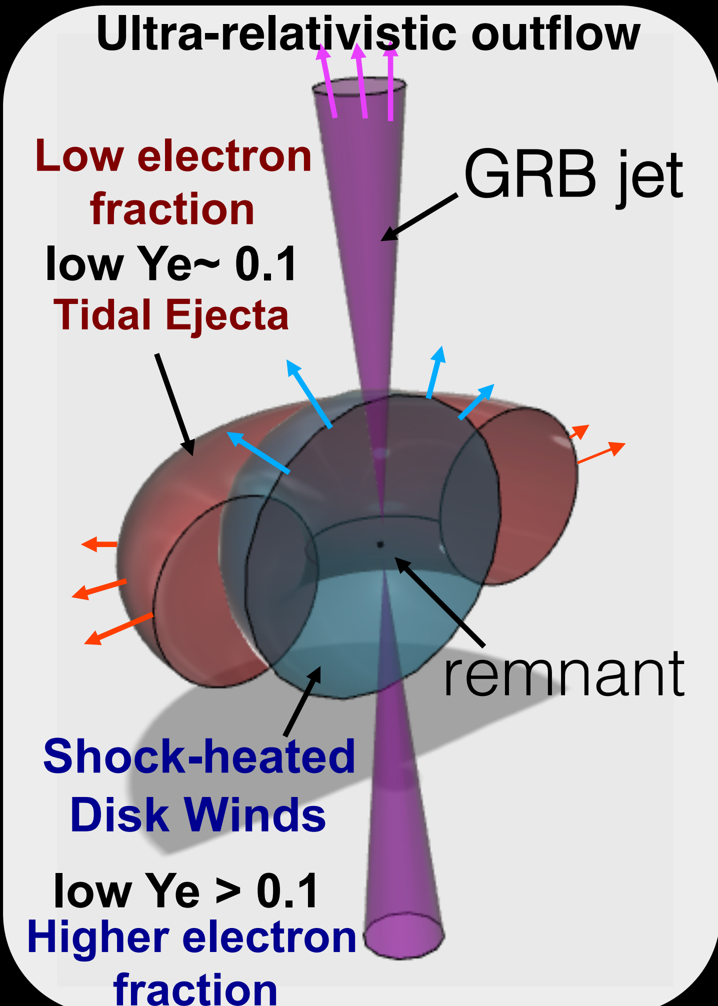

Courtesy of S. Ascenzi

Tidal Ejecta → **Red Macronova "equatorial"**

unbound by hydrodynamic interaction and gravitational torques

Peaks at days - 1 week after the merger

Secular – isotropic

accretion disk matter unbound by viscous and nuclear heating

Shock-heated → **Blue Macronova "Polar"**

squeezed matss at NS contact interface ejected by remnant pulsations

Peaks at 1-2 day after the merger

Disk Winds

neutrino absorption or magnetically launched winds

Observables: expectations

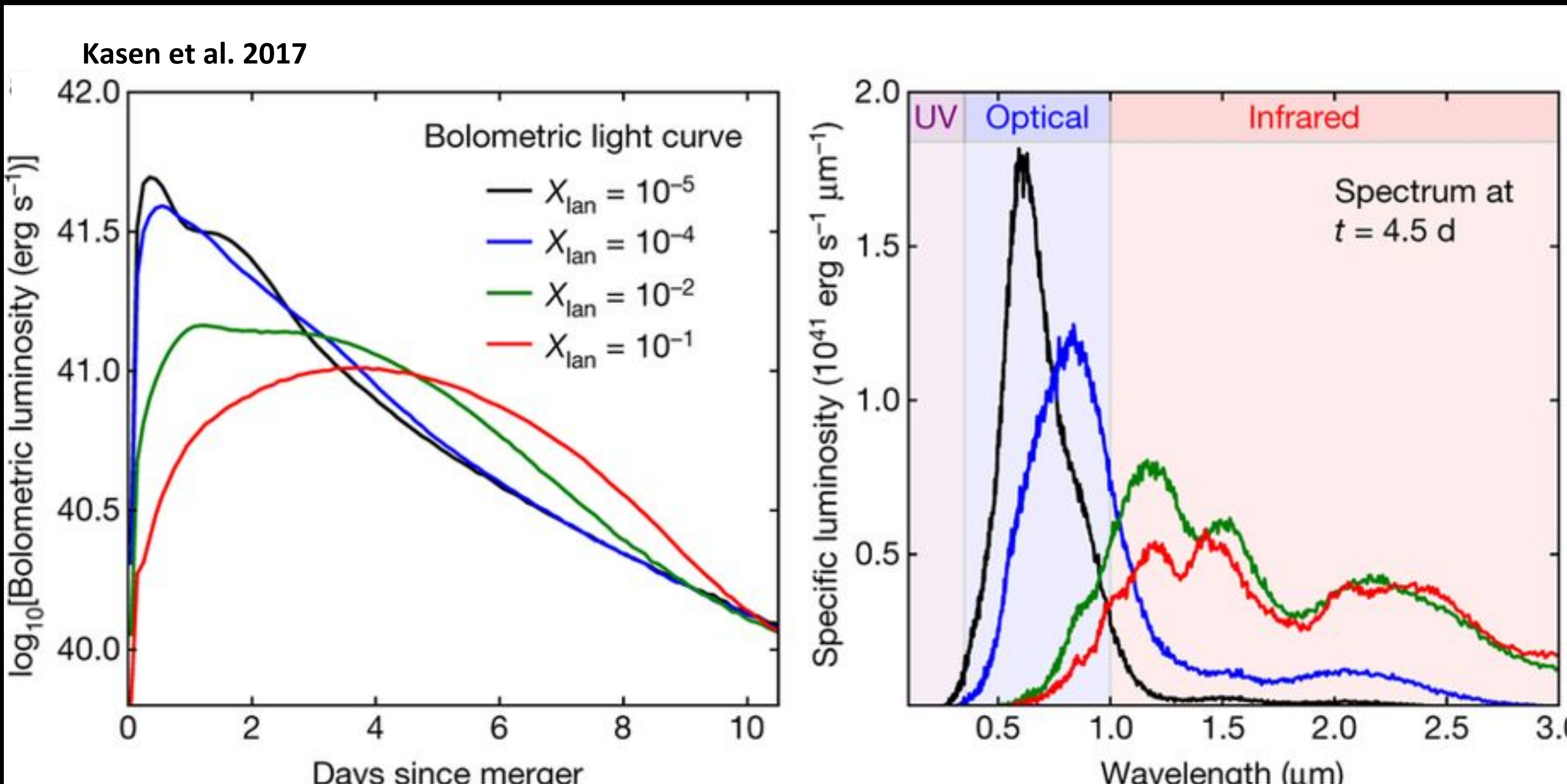

Light curve shape (duration and peak luminosity) and spectarl shape are dramatically affected by lanthanides

UV/Optical/NIR Light Curves

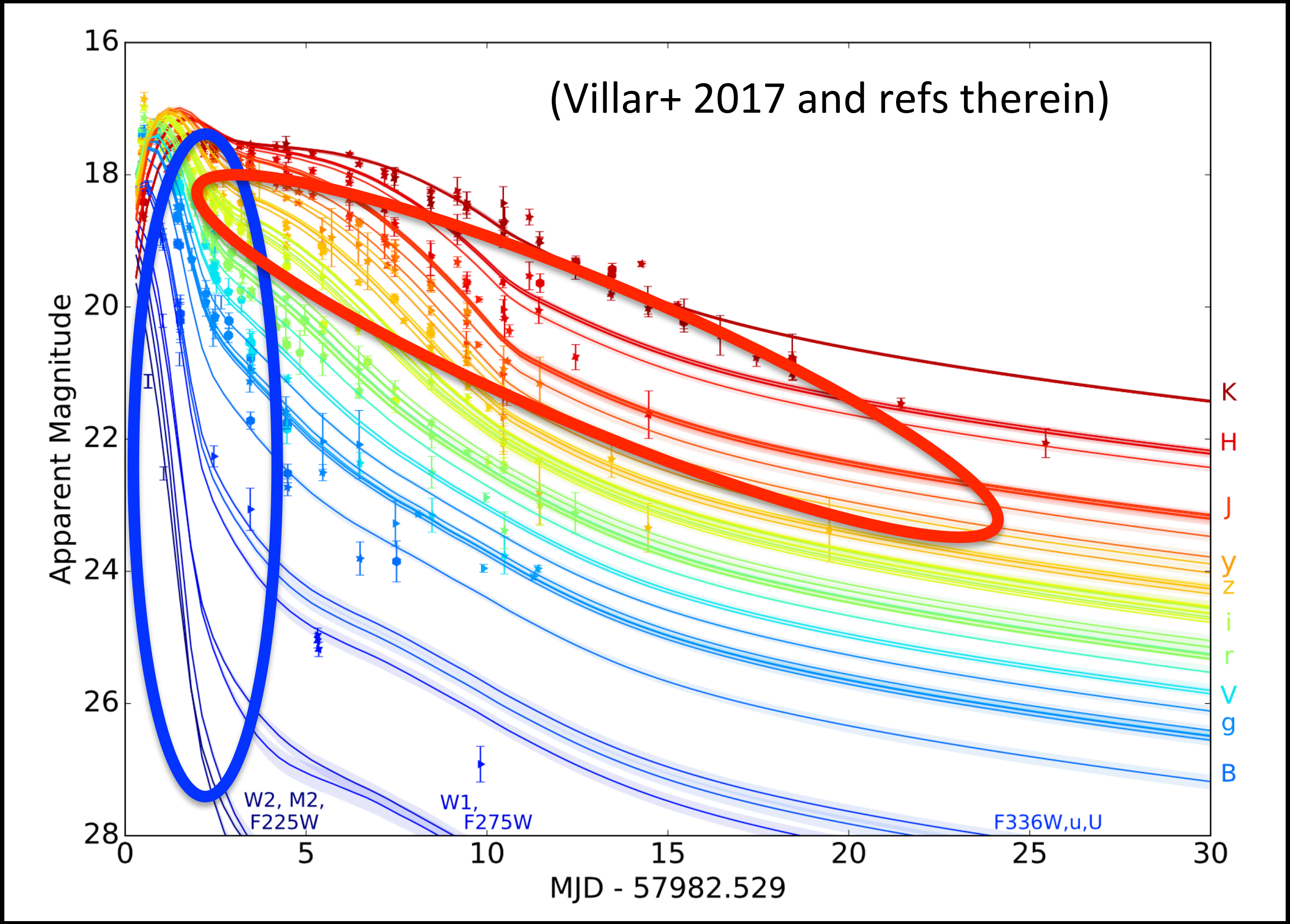

Extremely well characterized photometry of a Kilonova:

thermal emission by radiocative decay of heavy elements synthesized in multicomponent (2-3) ejecta!

ESO-VLT/X-Shooter

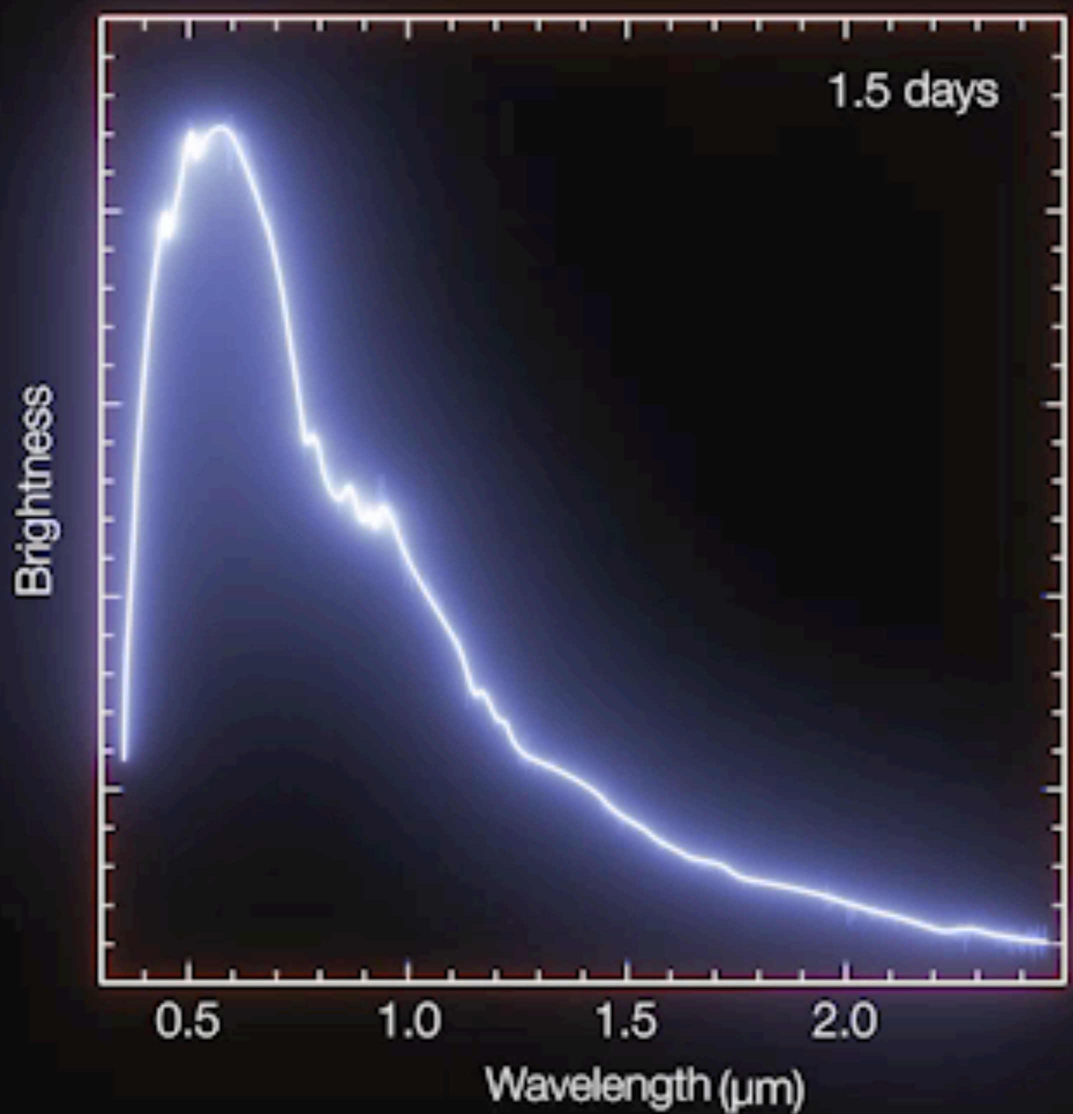

First spectral identification of the kilonova emission

- the data revealed signatures of the radioactive decay of **r-process nucleosynthesis**

(Pian et al. 2017, Smartt et al. 2017)

- BNS merger **site for heavy element production in the Universe!**

(Cote et al. 2018, Rosswog et al. 2017)

Credit: ESO/E. Pian et al./S. Smartt & ePESSTO/L. Calçada

The Kilonova AT2017gfo associated to GW170817

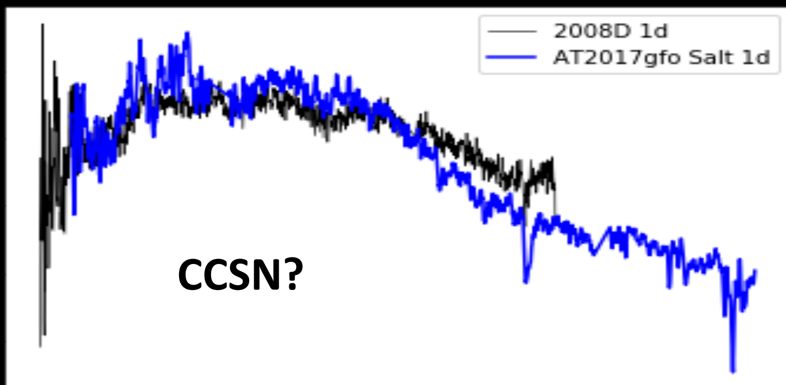

Buckley et al. 2017 MNRAS, McCully et al. ApJL

The low S/N optical spectrum at 1d matches very well that of SN2008D/ XRF080109 at similar phase

There is **no evidence** for a kilonova

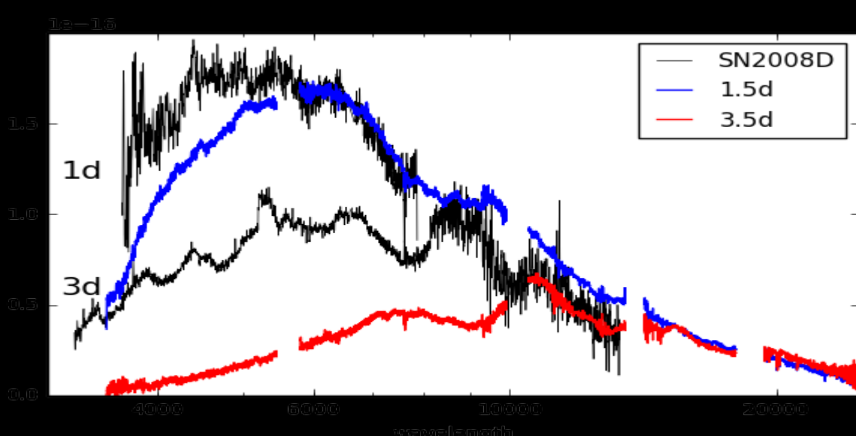

In a couple of days the peak of the spectral energy distribution shifts to the near infrared. Broad spectral features appear that are completely different from that of all know SN types

Spectroscopy: chemical signatures are hidden by kinematics

CARTOON

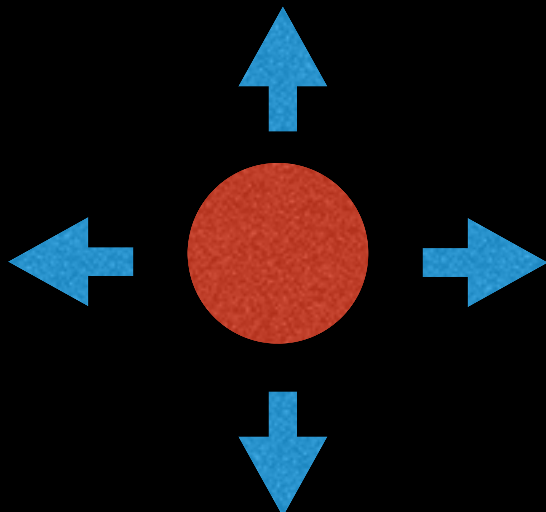

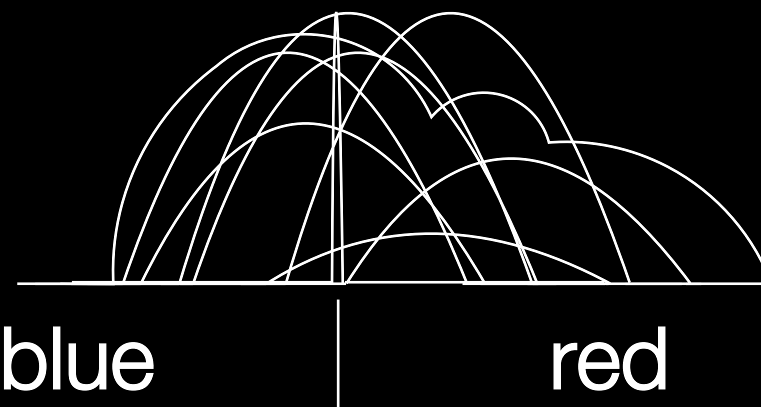

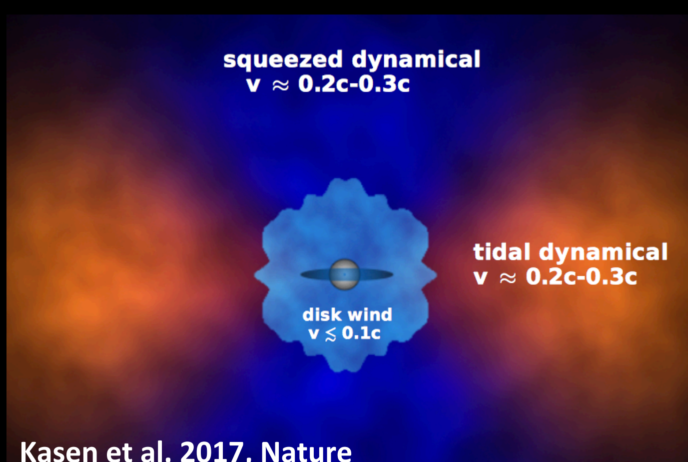

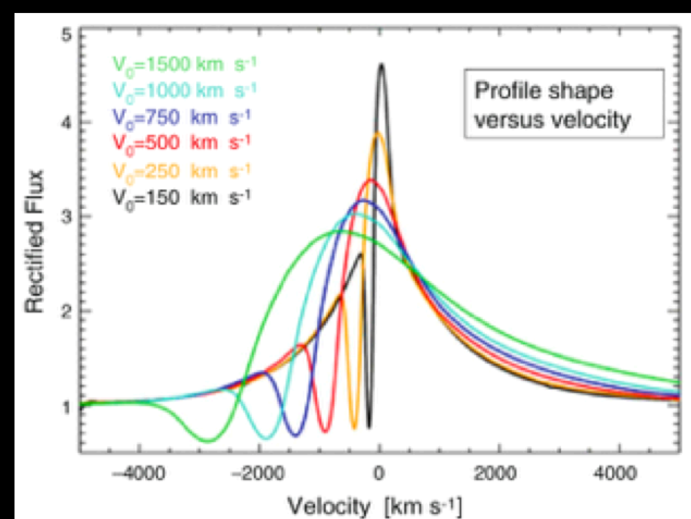

Credit: E. Cappellaro

NUCLEOSYNTHESIS

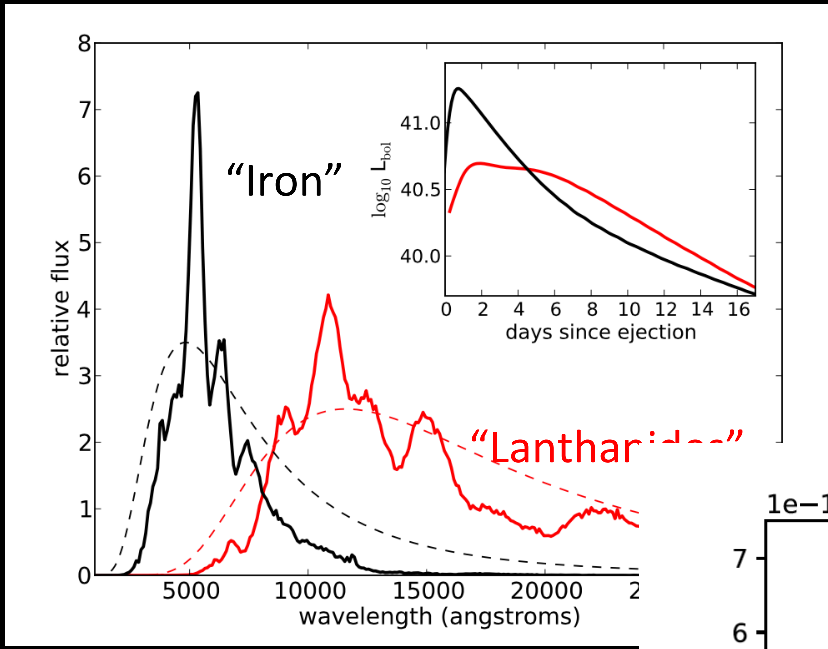

Kasen et al. 2013

Kilonova models predict the emergence of broad features of r-process elements

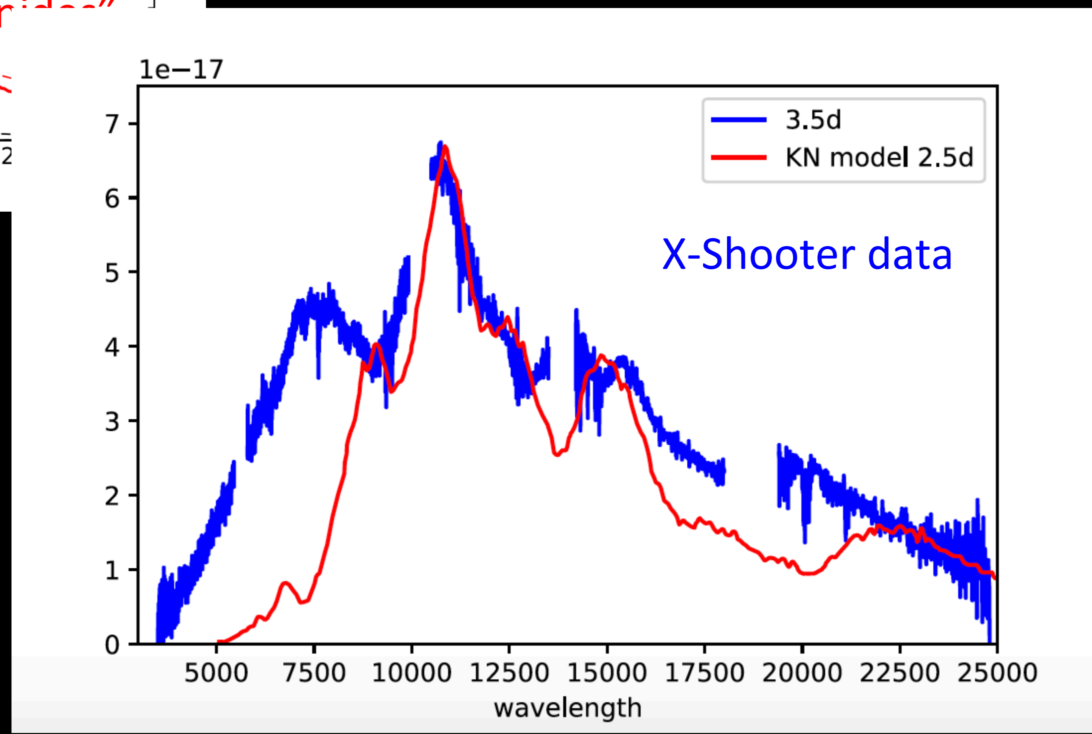

Basic parameters

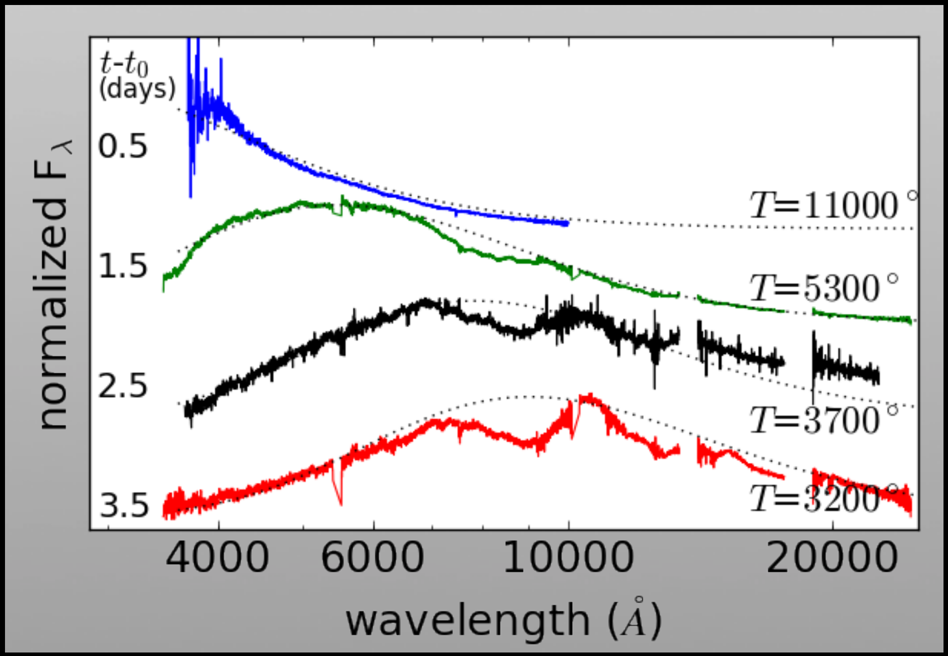

Drout et al. 2017

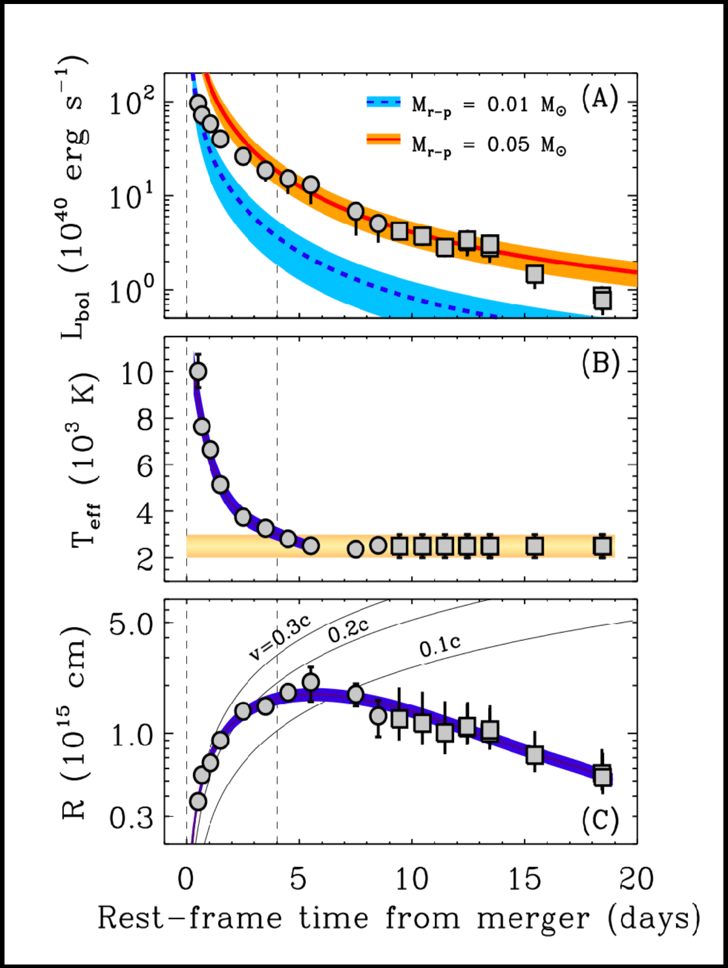

1) Bolometric luminosity decline

Very rapid expansion and cooling in 4 days

2) Then remains temperature almost constant

→ **EJECTED MASS ~ 0.03 – 0.05 $M_\odot$**

→ **EXPANSION VELOCITY IS OF 0.3 -0.1 C**

BASIC PHYSICAL PARAMETERS DERIVED FROM THE ULTRAVIOLET TO NEAR-INFRARED KILONOVA EMISSION

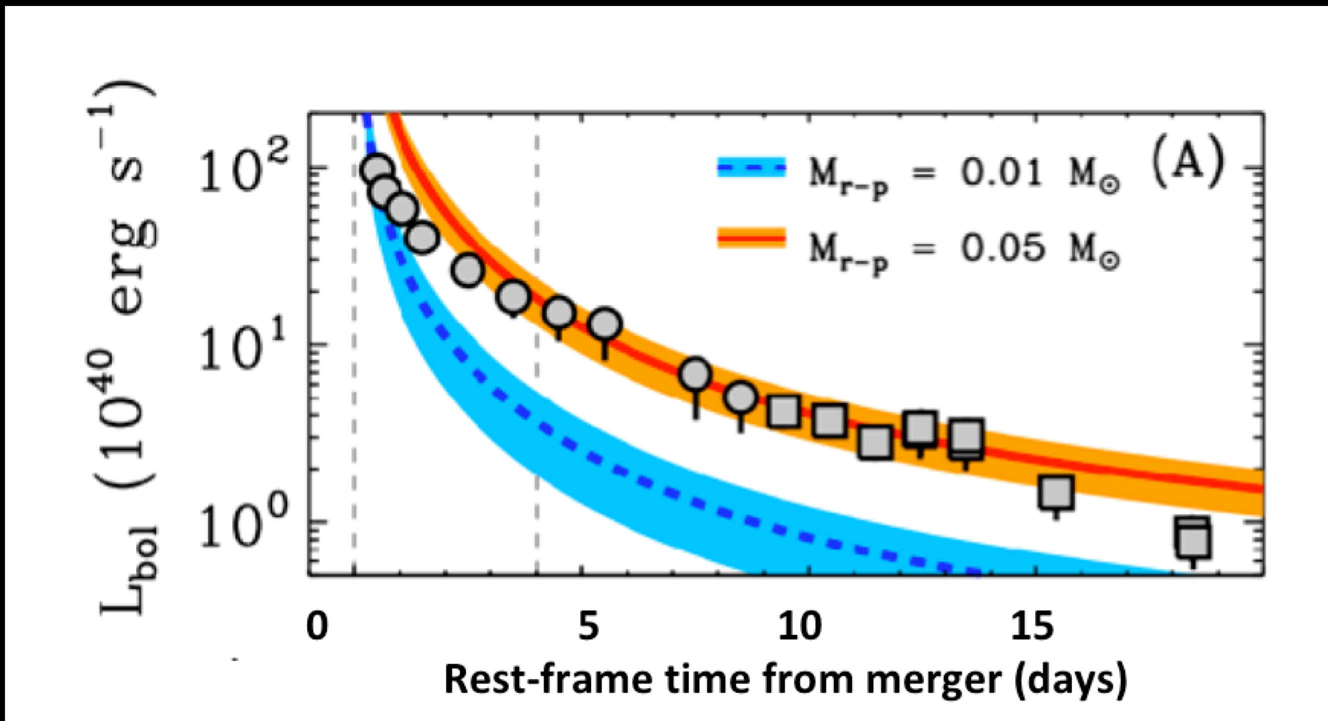

$$L_r = \epsilon_{\rm th} \dot{q}_r M_r$$

HEATING RATE

$$\dot{q}_r = 3 \times 10^{10} t_{\rm day}^{-1.3}\ {\rm erg\,s^{-1}\,g^{-1}}$$

THERMALIZATION EFFICIENCY

$$\epsilon_{\rm th} = 0.36 \left[\exp(-a t_{\rm day}) + \frac{(1 + 2bt^d)}{2bt^d_{\rm day}} \right]$$

BASIC PHYSICAL PARAMETERS DERIVED FROM THE ULTRAVIOLET TO NEAR-INFRARED KILONOVA EMISSION

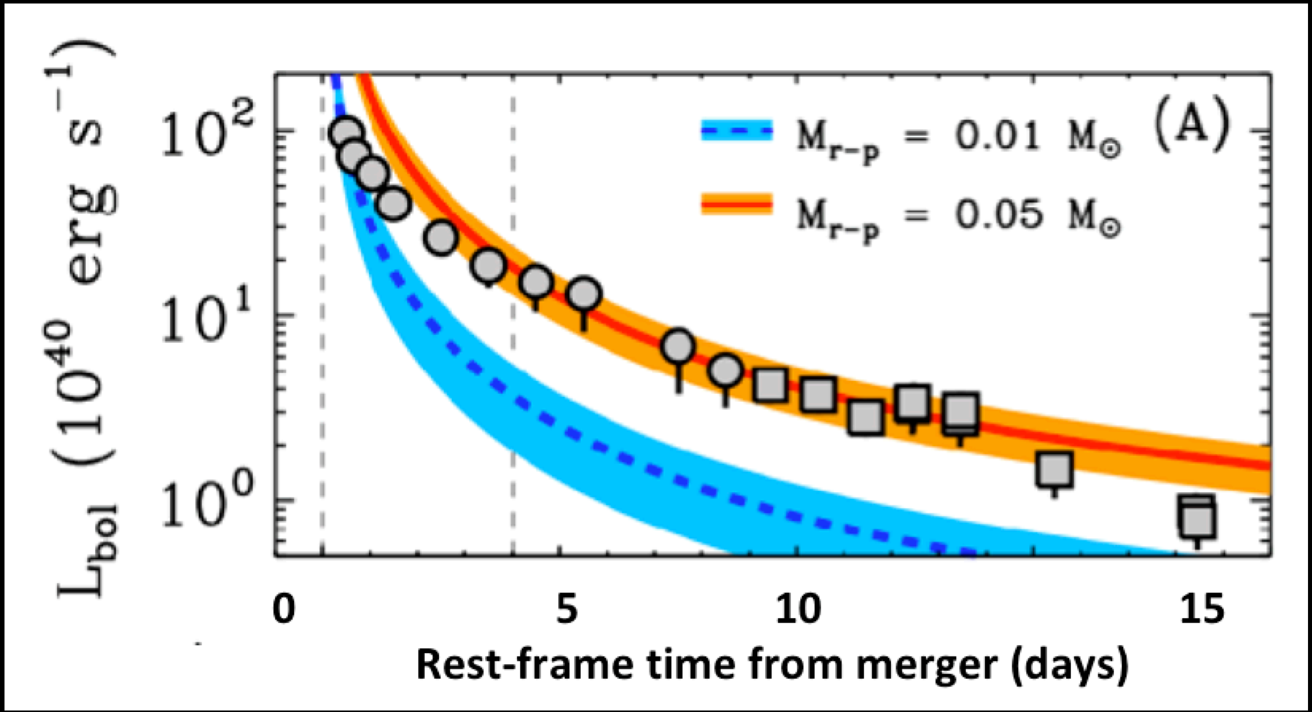

- REPRESENTATIVE R-PROCESS RADIOACTIVE HEATING CURVES:

~0.01 $M_\odot$ of r-process material (blue curve) −EARLY TIME

~0.05 $M_\odot$ of r-process material (red curves) – LATE TIME

Stefan-Boltzman law relates bolometric luminosity, surface area, and temperature

$$L = 4\pi R^2 \sigma T_e{}^4$$

BEST-FITTING BLACK-BODY MODEL TEMPERATURES

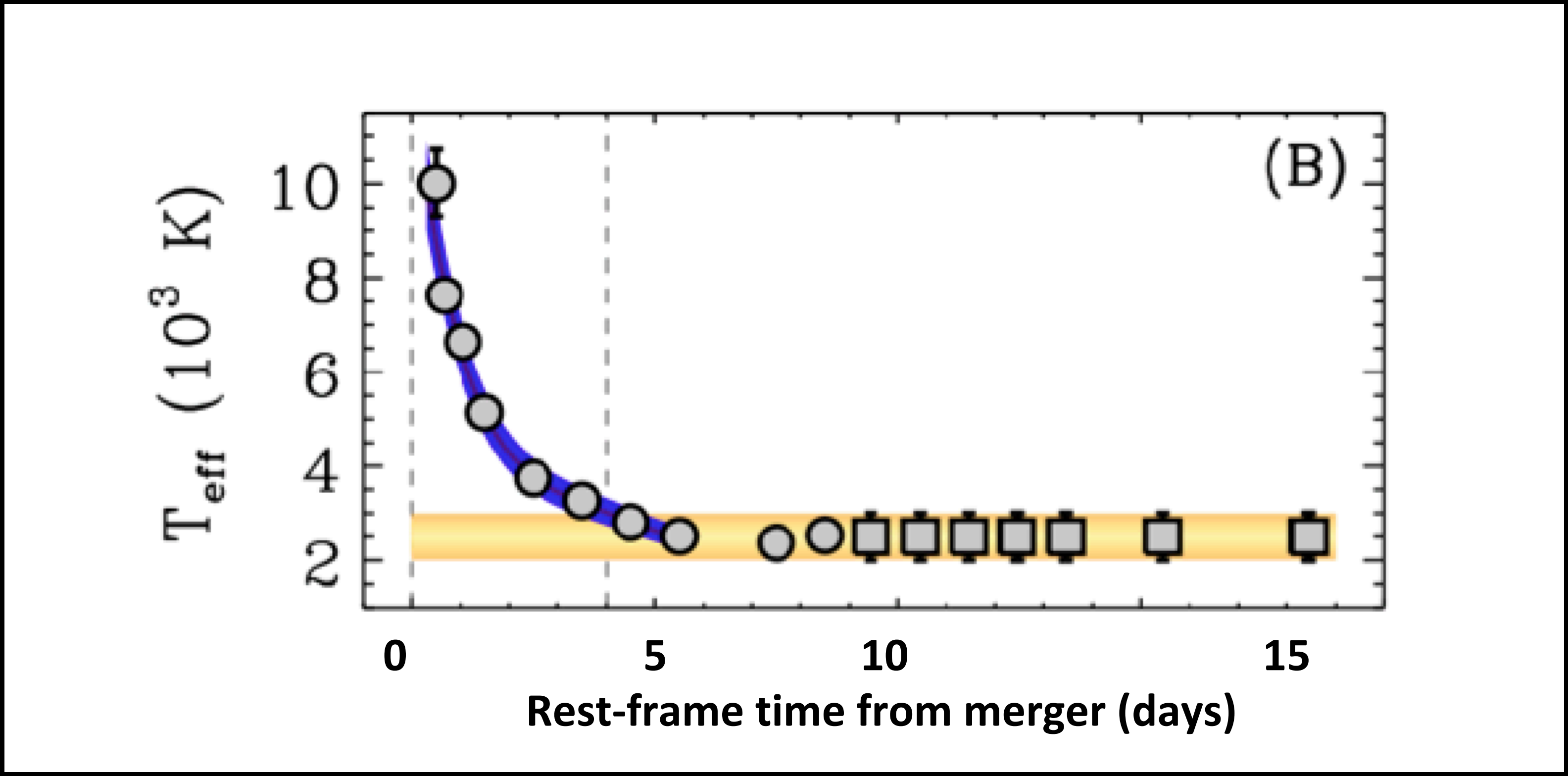

- Between 4.5 and 8.5 days, the temperature asymptotically approaches ~2500K
- At 2500K→ recombination of open f-shell lanthanide elements, rapidly reduced opacity and photsphere move inward (square in the plot)

BEST-FITTING BLACK-BODY MODEL RADII

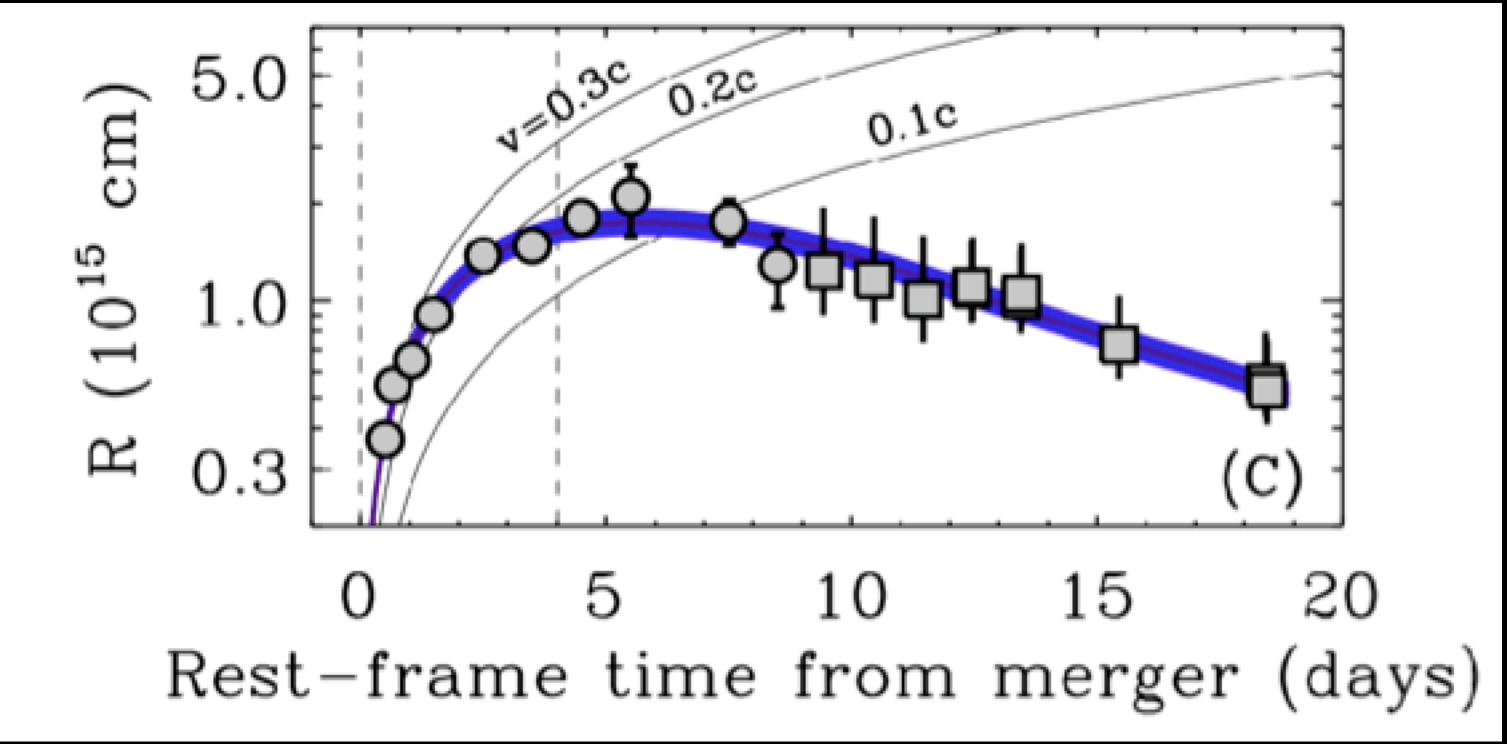

- Curved lines represent the radius of material moving at 10%, 20%, and 30% the speed of light.
- First days the radius increase with time implies that the ejecta (photosphere) expands at relativistic speeds
- after about 5 days, the measured radii decrease, likely due to recombination the photosphere begins moving inward.

Multi-component kilonova emission (Pian et al. 2017, Nature,551, 57)

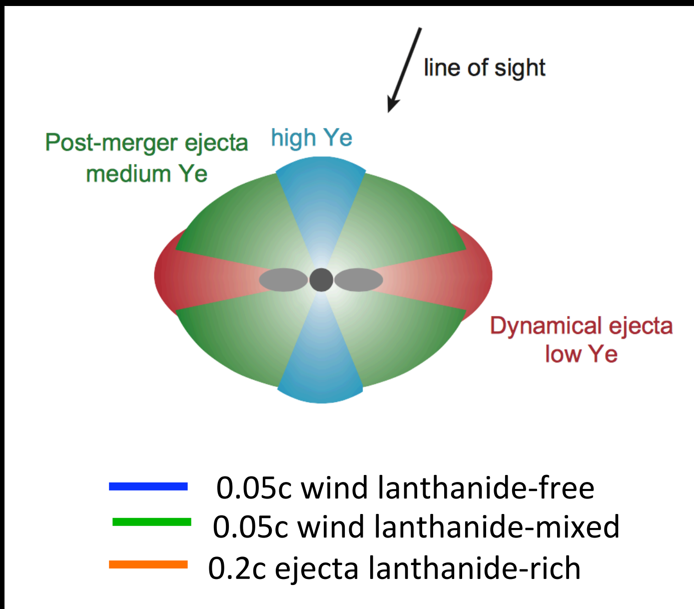

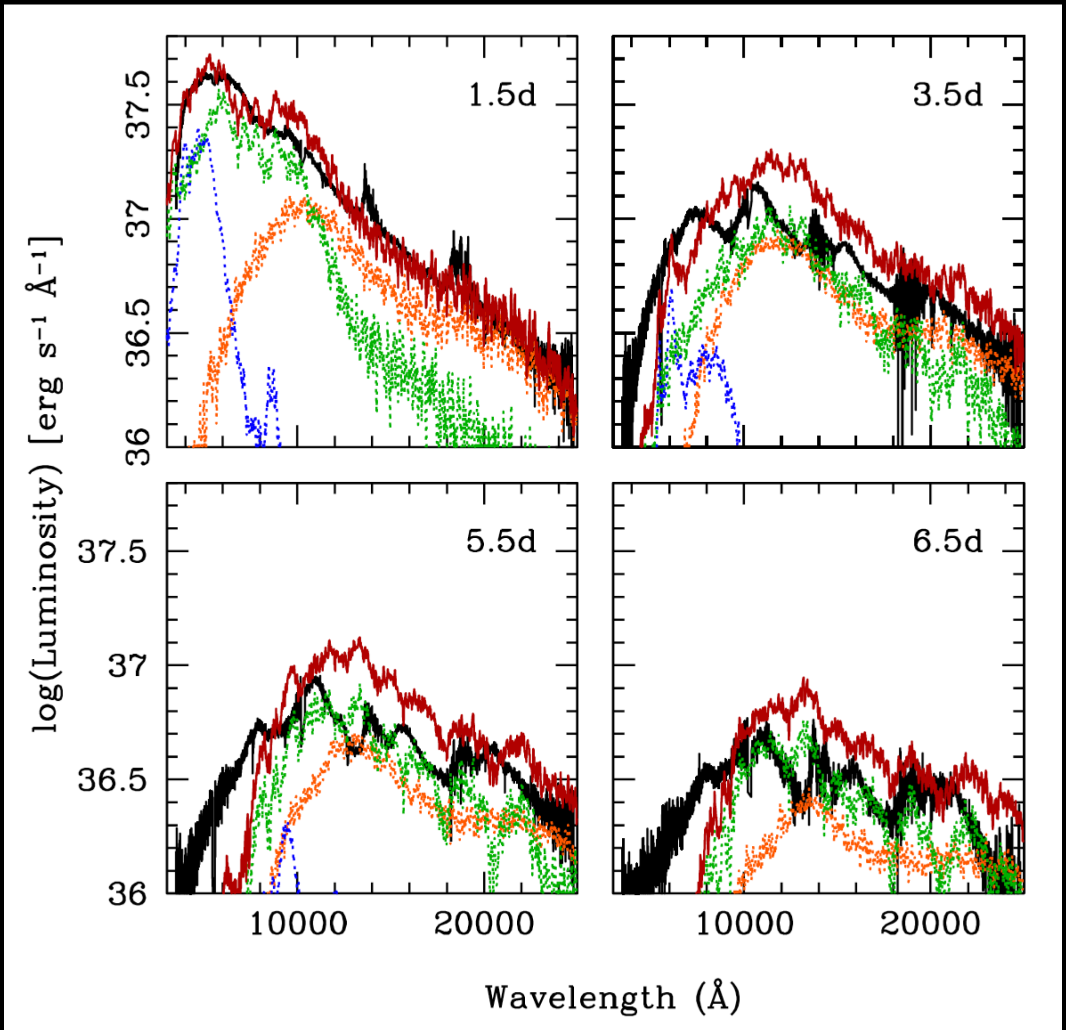

Best fit requires three components

ejected mass ~ 0.03 – 0.05 $M_{\odot}$

At present models are not able to reproduce consistently all the observed spectral features

ESO-VLT/X-Shooter

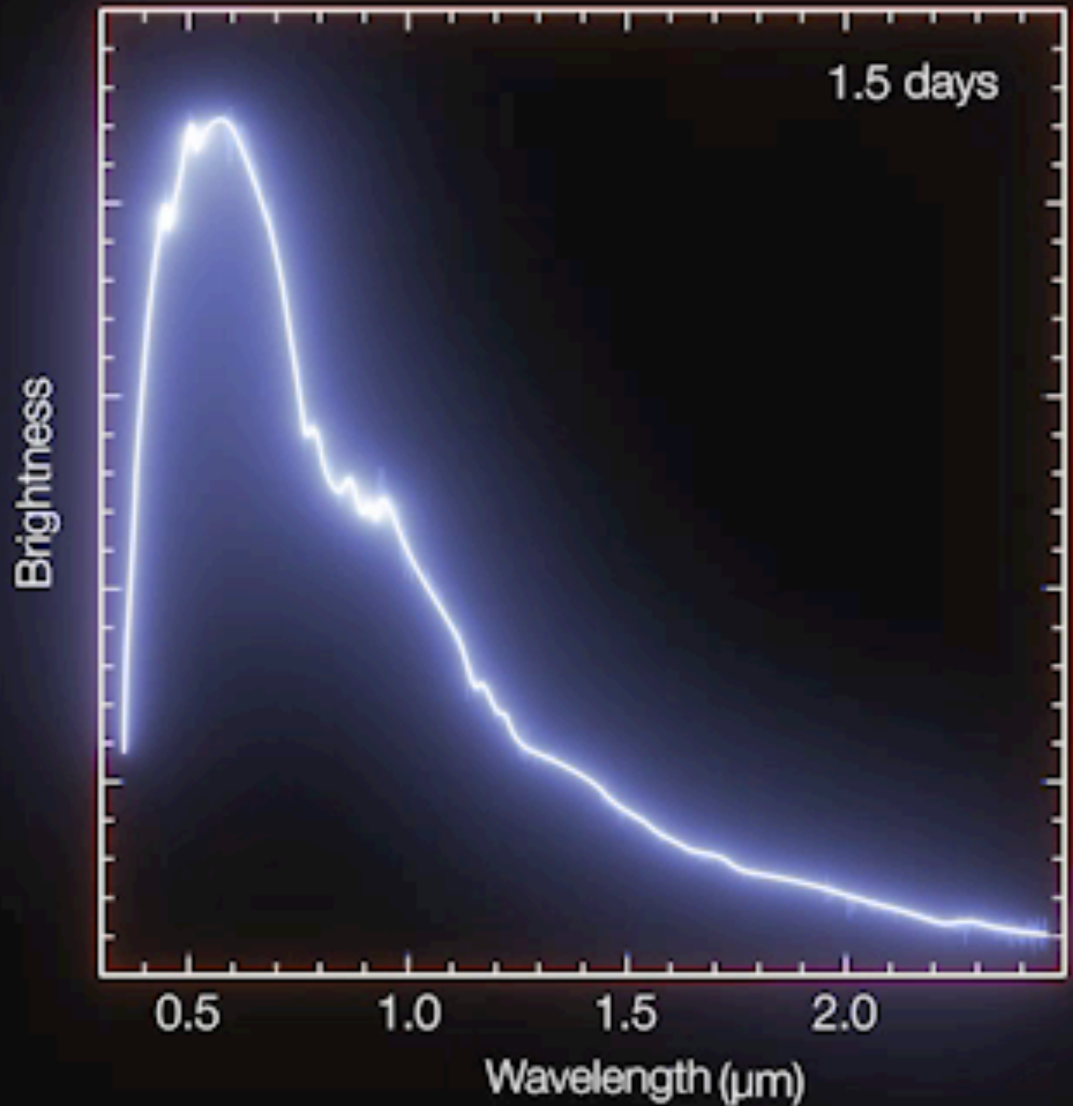

Credit: ESO/E. Pian et al./S. Smartt & ePESSTO/L. Calçada

Possible signatures of Cesium and Tellurium

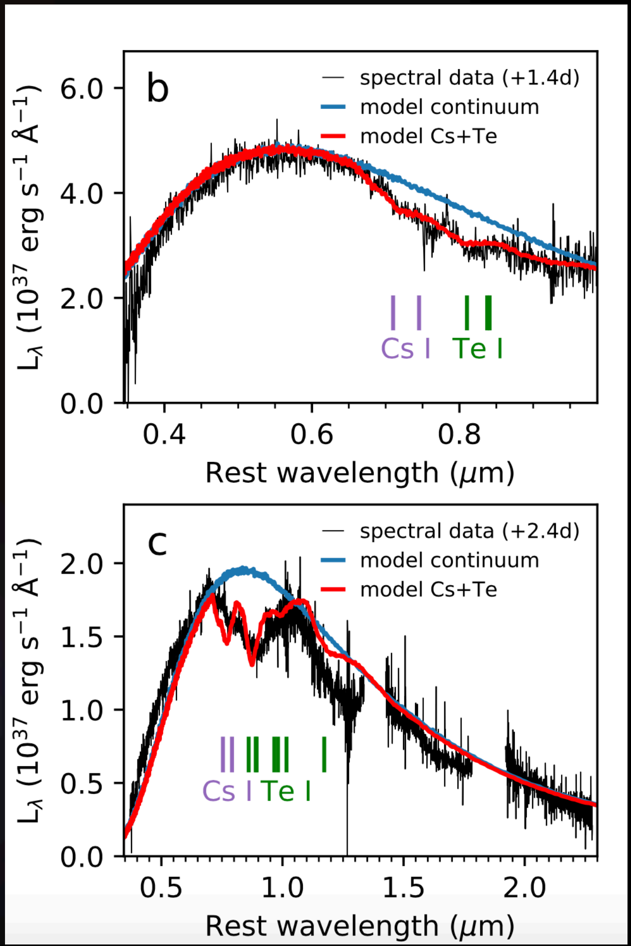

Smartt et al. 2017, Nature

Nucleosynthesis

Smartt et al. 2017

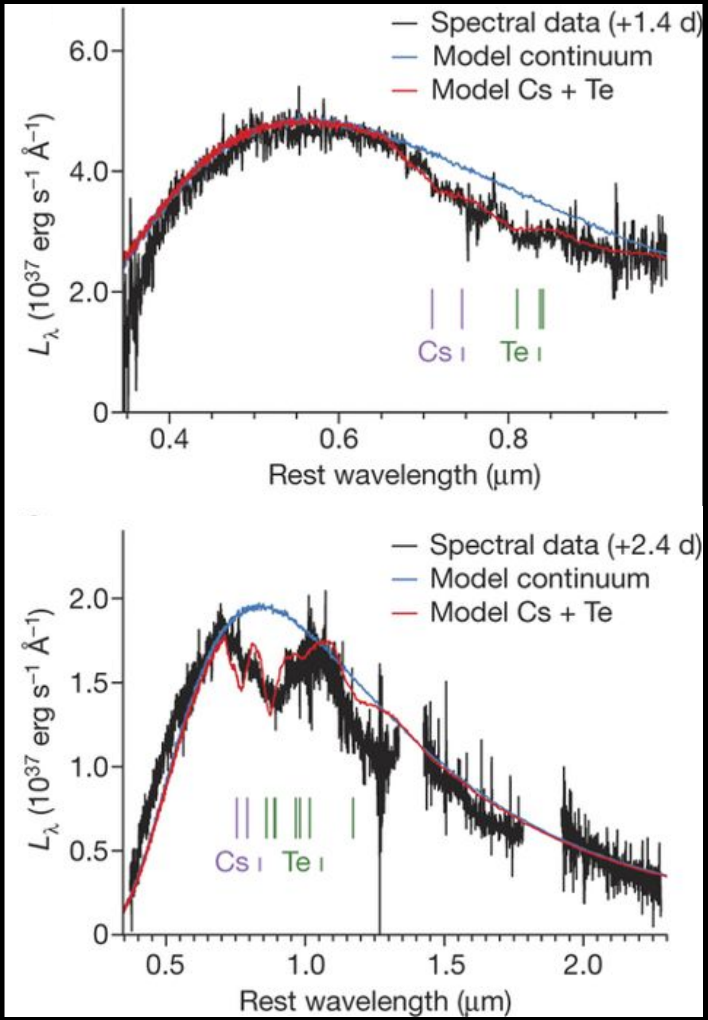

Spectral analysis hampered because of:

- heavy elements have forest of lines hence strong blending
- relativistic velocity makes for extremely broad lines (multi-components and different velocities)
- atomic data are incomplete and uncertain

Attempt to identify elements

Neutral caesium

Excited tellurium

(Gold has no optical lines ☹)

A recent work…

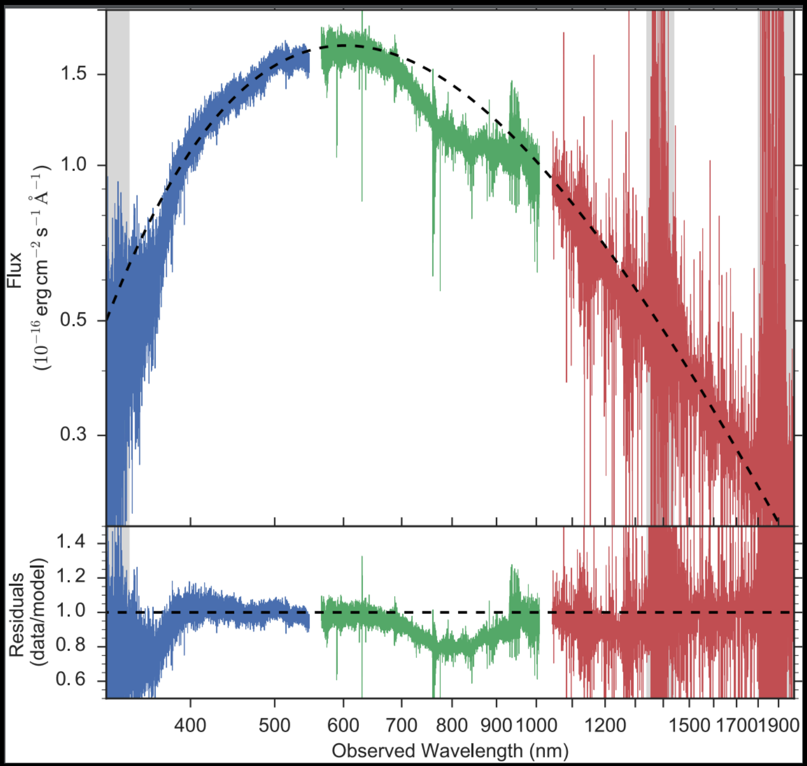

Watson, D. et al. accepted in Nature

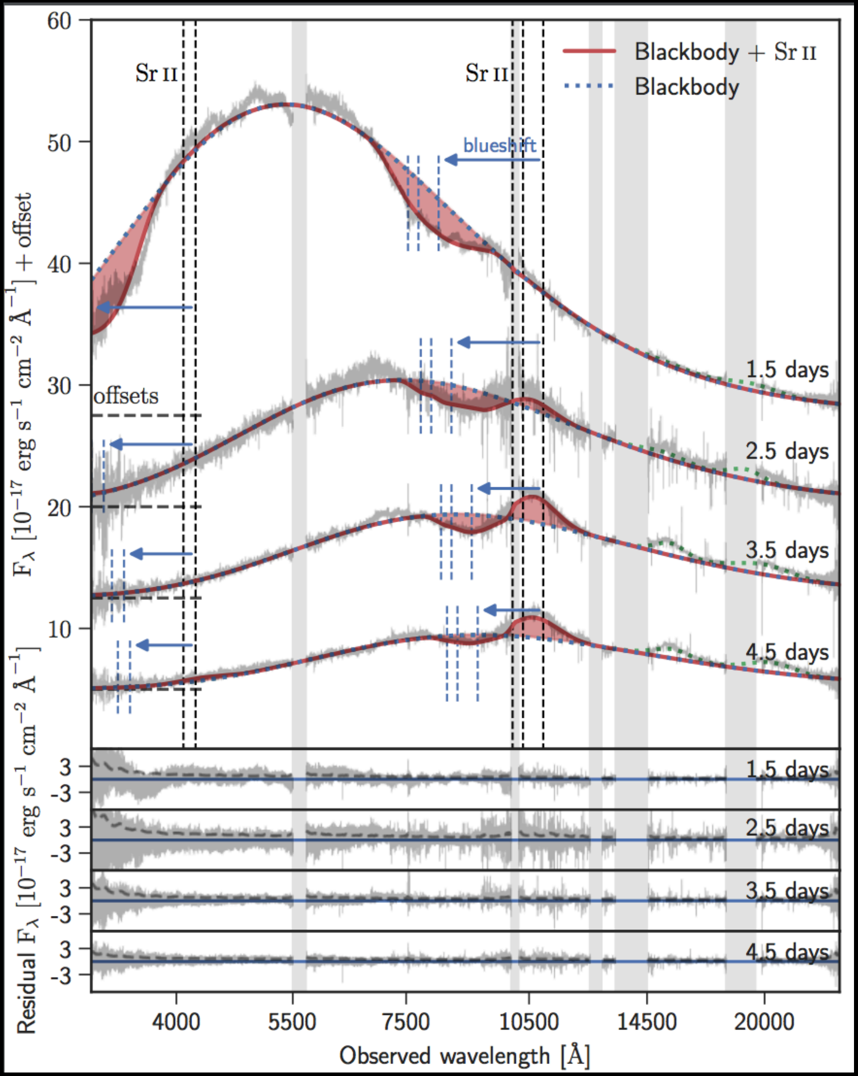

identification of the neutron-capture element **strontium**

Media press..

THE BINARY NEUTRON STAR MERGERS IS A COSMIC MINE
FORGING ABOUT 100 EARTH-MASSES OF HEAVY GOLD

INFERRED RATE FROM GW170817 EXPLAIN R-PROCESS ELEMENTS ABOUNDANCE

R_{BNS}=320-4740 $Gpc^{-3}\ yr^{-1}$

LVC 2017 PhRvL,119

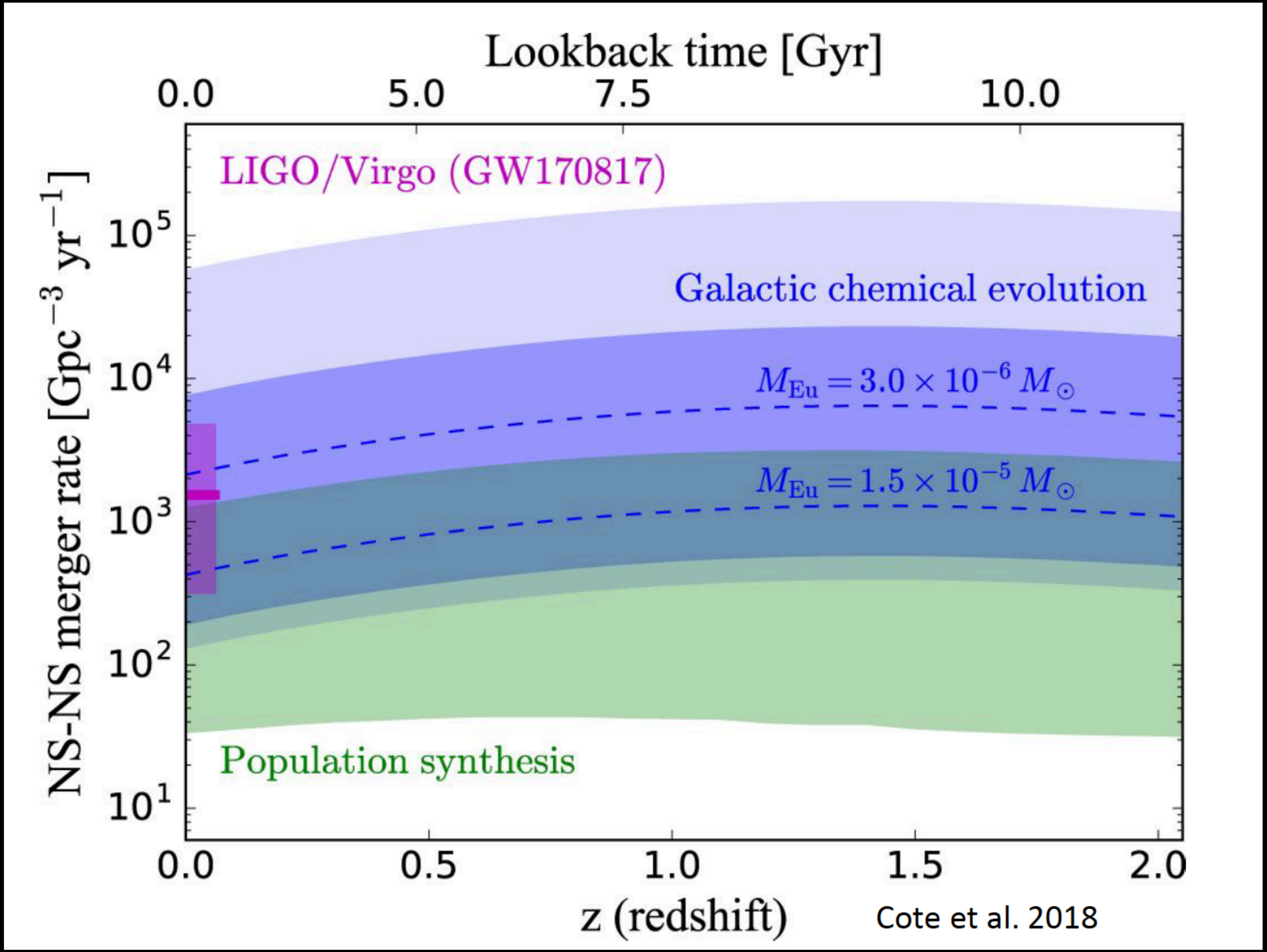

Multi-messenger studies

GRB/GW FUNDAMENTAL PHYSICS/COSMOLOGY

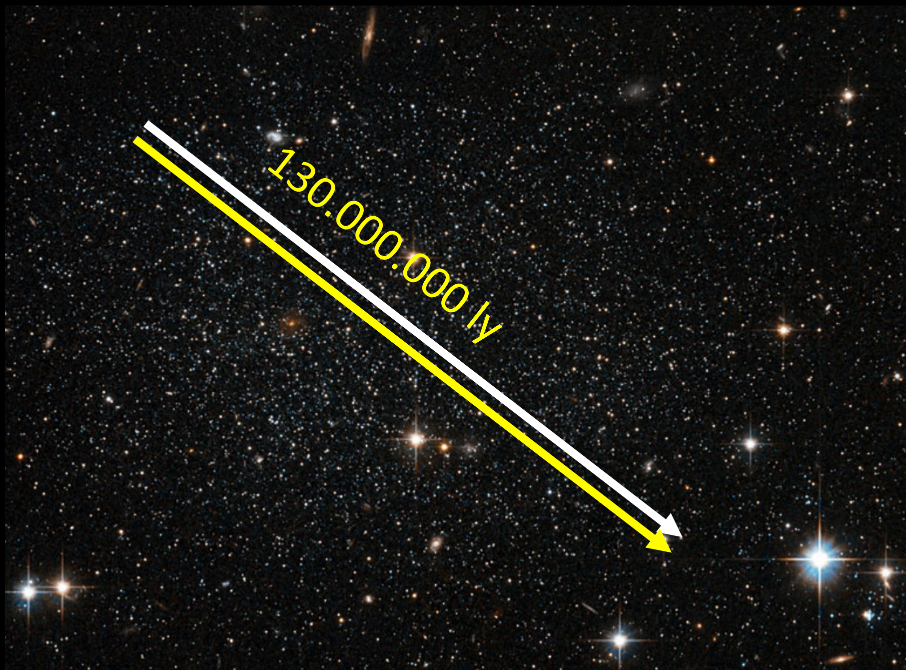

GRB/GW delay

$$\Delta t = (1.74 \pm 0.05)\, s$$

and 40 Mpc distance
→ difference speed of gravity and speed of light between

$$-3 \times 10^{-15} \leqslant \frac{\Delta v}{v_{\mathrm{EM}}} \leqslant +7 \times 10^{-16}$$

GWs propagate at the speed of light to within $1{:}10^{15}$!

LVC 2017, APJL, 848, L13

Consequences of multi-messenger detection of GW170817 for cosmology →
Constraint on the speed of GWs ruled out many classes of modified gravity models
(quartic/quintic Galileons, TeVeS, MOND-like theories, see, e.g., Baker et al. ’17, Creminelli & Vernizzi ’17)

NGC4993 Host galaxy

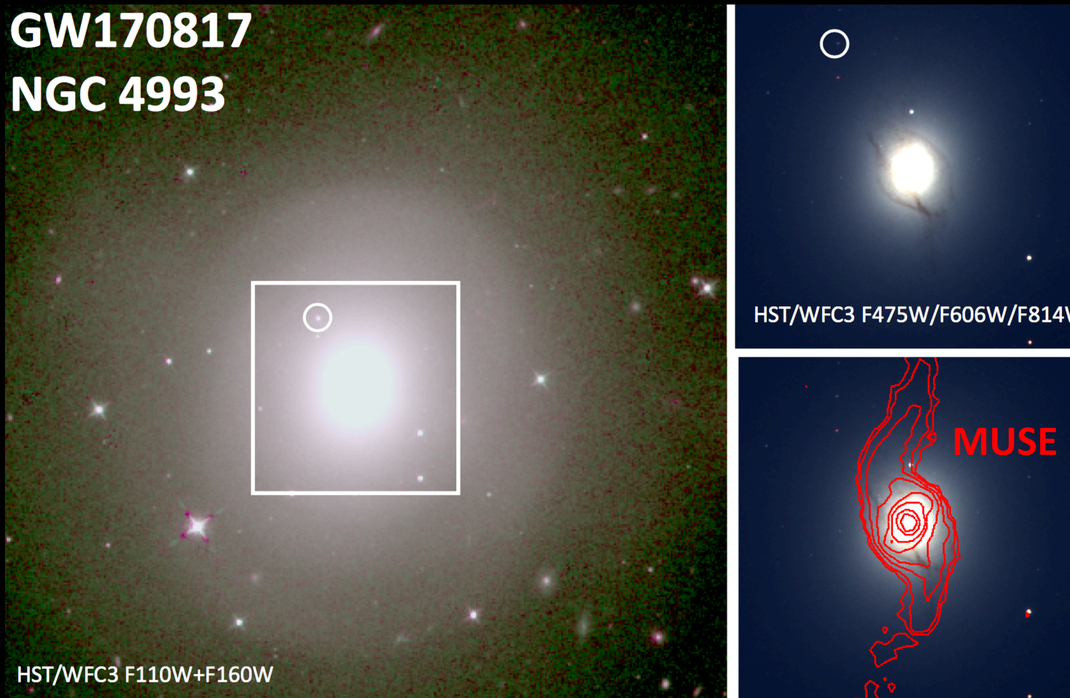

Levan et al. 2017, ApJL, 848

log(M*/Msol) ~10.65
Median age ~ 11.2 Gyr
SFR ~ 0.01 Msol yr^{-1}

Blanchard et al. 2017

S0 galaxy at z = 0.009783

- Face-on spiral shells and edge-on spiral features → **recent (< 1 Gyr) galaxy merger**
- HST imaging → **no globular or young stellar clusters**
- **Old population** in the vicinity of GW source
- Age and offset from the galaxy center → **small natal kick velocity**

(Levan et al. 2017; Pan et al. 2017; Kasliwal et al. 2017; Im et al. 2017)

COSMOLOGY →HUBBLE DIAGRAM

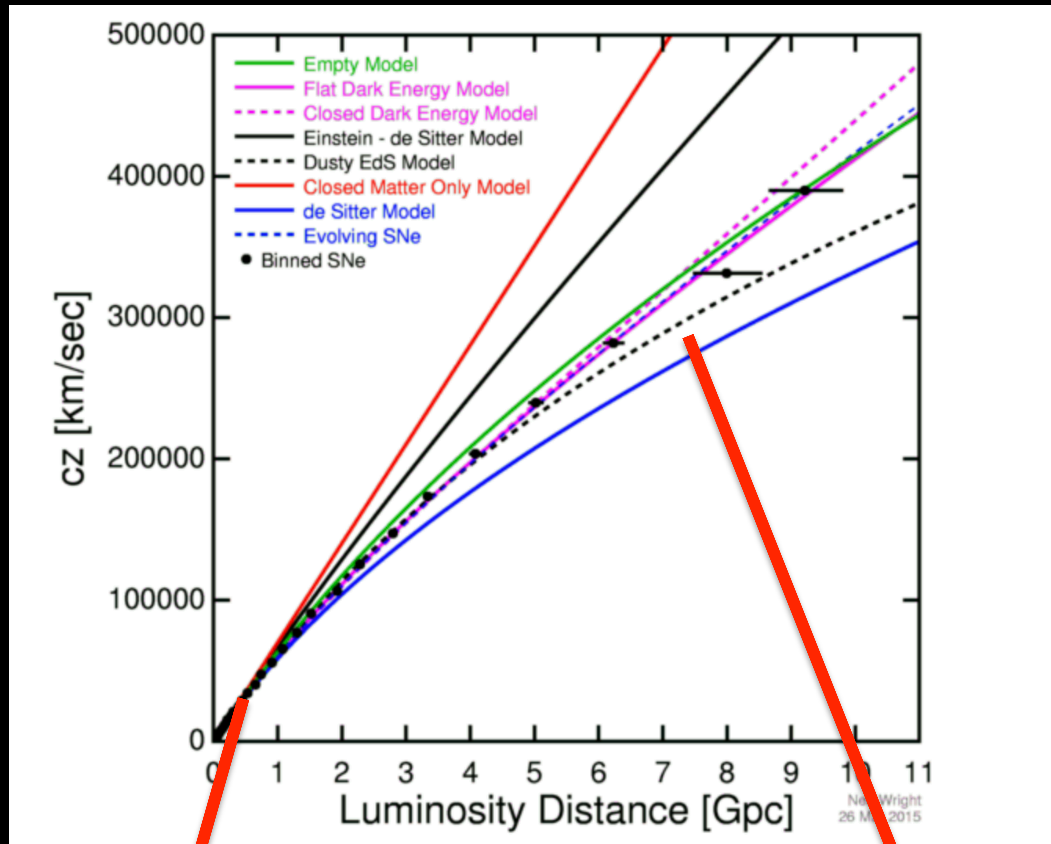

slope of the trend determines present normalized expansion rate, the LOCAL HUBBLE COSTANT H0

shape of the trend at large redshifts determines the global GEOMETRY OF THE UNIVERSE

Observations to determine z - dL(z), which depends on cosmology via H(z)

$$d_L(z) = c\,(1+z)\int_0^z \frac{1}{H(z')}dz'$$

GRAVITATIONAL-WAVE COSMOLOGY

Independent determination of the present-day expansion rate of the Universe, using binary system as STANDARD SIREN (Schutz Nature1986)

GWs from binary inspiral as measured in a single detector

$$h_+ = \frac{2(1+z)\mathcal{M}}{D_L}[\pi(1+z)\mathcal{M}f]^{2/3}(1+\cos^2\iota)\cos 2\Phi_N(t),$$

$$h_\times = -\frac{4(1+z)\mathcal{M}}{D_L}[\pi(1+z)\mathcal{M}f]^{2/3}\cos\iota\sin 2\Phi_N(t),$$

Lowest order contribution to the orbital phase

Frequency

Chirp mass

$$\Phi_N(t) = \Phi_c - \left[\frac{t_c - t}{5(1+z)\mathcal{M}}\right]^{5/8}$$

$$f \equiv \frac{1}{\pi}\frac{d\Phi_N}{dt}$$

$$\Phi_N(t) = \Phi_c - \left[\frac{t_c - t}{5(1+z)\mathcal{M}}\right]^{5/8}$$

$$(1+z)\mathcal{M}$$

$$h_+ = \frac{2(1+z)\mathcal{M}}{D_L}[\pi(1+z)\mathcal{M} f]^{2/3}(1+\cos^2\iota)\cos 2\Phi_N(t),$$

$$h_\times = -\frac{4(1+z)\mathcal{M}}{D_L}[\pi(1+z)\mathcal{M} f]^{2/3}\cos\iota\sin 2\Phi_N(t),$$

D_L

Standard Siren → absolute calibration

But require independent z determination, e.g EM counterpart

GRAVITATIONAL-WAVE COSMOLOGY

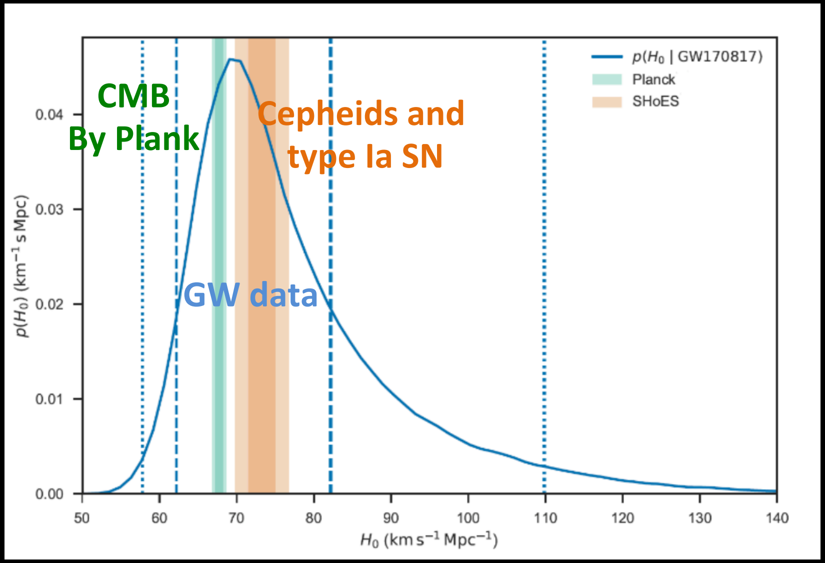

Recession velocity /redshift

GW distance

$$v_H = H_0 d$$

Combining the distance measured from GWs

$$d = 43.8^{+2.9}_{-6.9}\,\mathrm{Mpc}$$

and NGC4993 recession velocity

$$\rightarrow H_0 = 70.0^{+12.0}_{-8.0}\,\mathrm{km\,s^{-1}\,Mpc^{-1}}$$

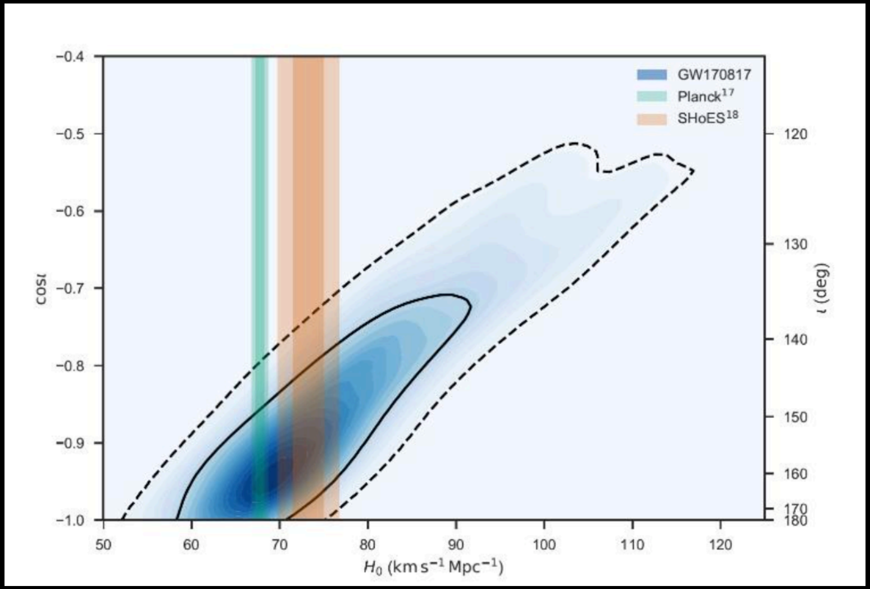

Abbott et al. 2017, Nature, 551, 85A

GRAVITATIONAL-WAVE COSMOLOGY

EM info improving GW H0 estimate:

- Break the degeneracy inclination/distance with **precise measure of the host galaxy distance** (e.g. Surface brightness fluctuation → distance error less then 5%, Cantiello+ 2017)

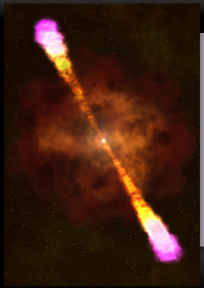

Using **inclination information from kilonova / afterglow models** (Hotokezaka+ 2018)

H0 statistical estimate, using **cross-correlation with potential host galaxies within the localization volumes**
(Chen+ 2017, arXiv:1712.06531, Fishbach+ arXiv:1807.05667)

NEUTRON STARS

Unique natural laboratories for studying behavior of cold, high-density nuclear matter.

Neutron Stars
Behavior is governed by equation of state (EoS), relationship between pressure and density:

- determines relation between NS mass and radius
- determines stellar moment of inertial
- determines tidal deformability

Thus measurement of NS masses, radii, moments of inertia and tidal effects provide information about EoS.

General relativity makes detailed predictions for the inspiral and coalescence of two compact objects, which may be neutron stars or black holes.

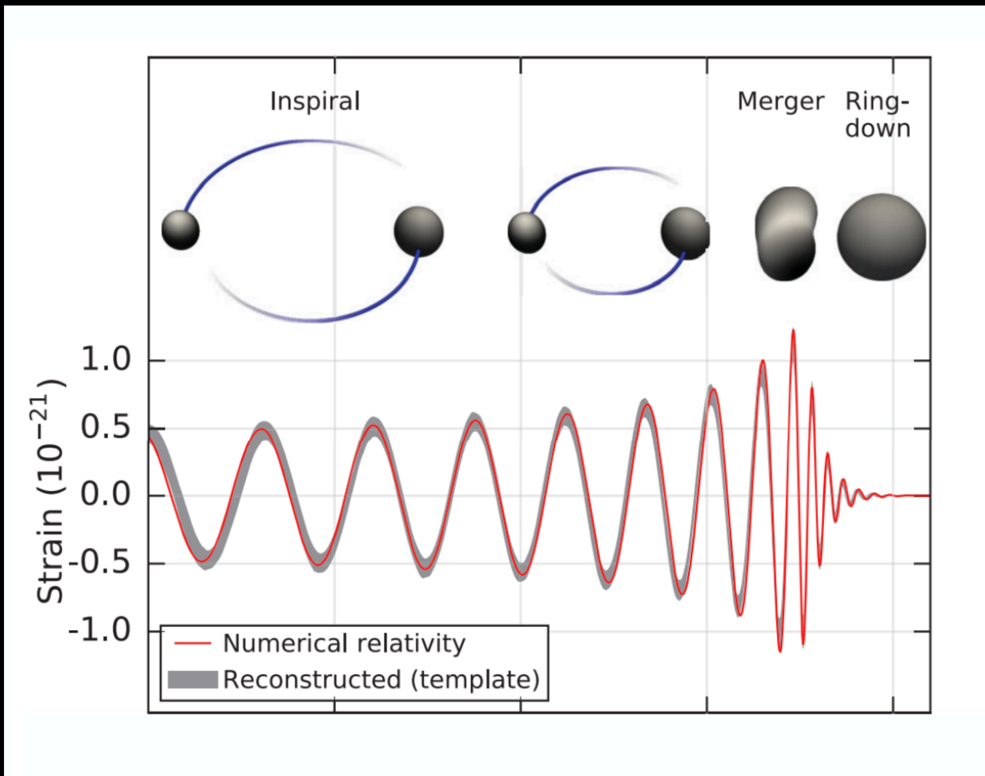

$$q = m_2/m_1, \text{ where } m_1 \geq m_2$$

EARLY INSPIRAL **LATE INSPIRAL**

$$\mathcal{M} = \frac{(m_1 m_2)^{3/5}}{(m_1 + m_2)^{1/5}}$$

1- Time evolution of the frequency is determined primarily by chirp mass

2- As the orbit shrinks and GW frequency grows rapidly

→ GW phase is increasingly influenced by relativistic effects related to the mass ratio, spin-orbit and spin-spin couplings

NS EFFECT ON GW SIGNAL

The objects' internal structure become important as the orbital separation approaches the size of the bodies

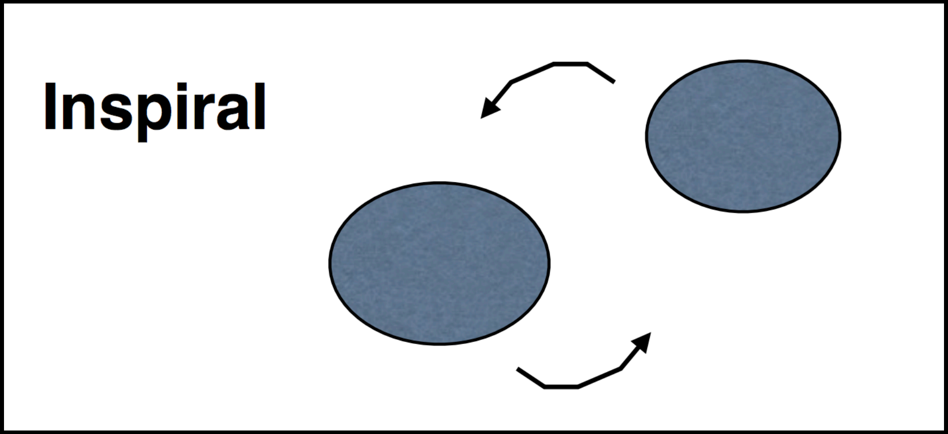

Tidal deformation of each star's gravitational field on its companion induces a mass-quadrupole moment and accelerates the coalescence

NS EFFECT ON GW SIGNAL

EoS affects GW behavior during merger and post-merger

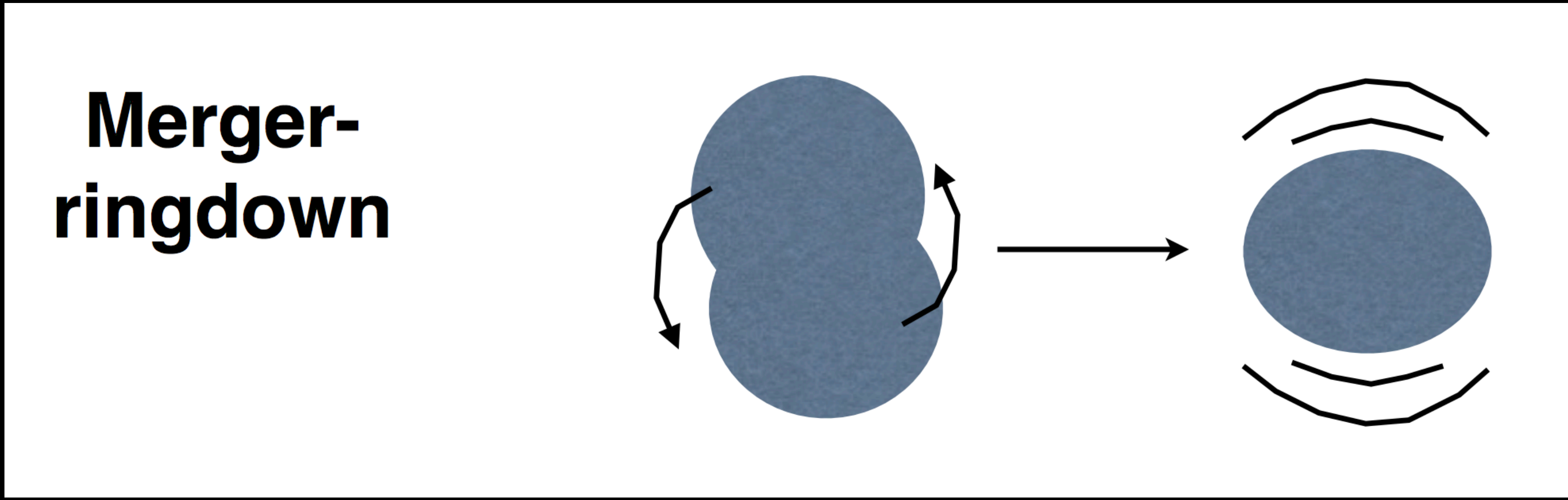

Merger and post-merger signal can provide lots of physics but signal is buried in the high noise at relevant frequencies

GW170817 PARAMETER ESTIMATION

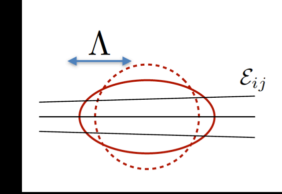

- We know the location! Fix location in sky.
- Assume two NSs with properties that are described by the same EoS
- Small spin prior in agreement with galactic binary NS spin measurements

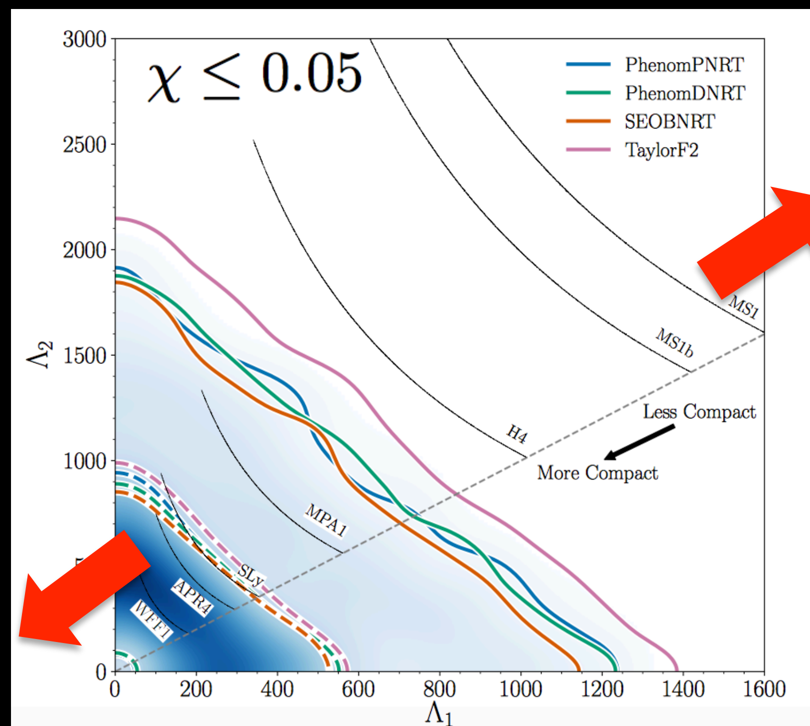

STIFF EOS: high maximum M and larger R for the same M (less compact)

SOFT EOS: low maximum M and smaller R for the same M (more compact)

Multimessenger constraints on nuclear EOS

Simulations in NR

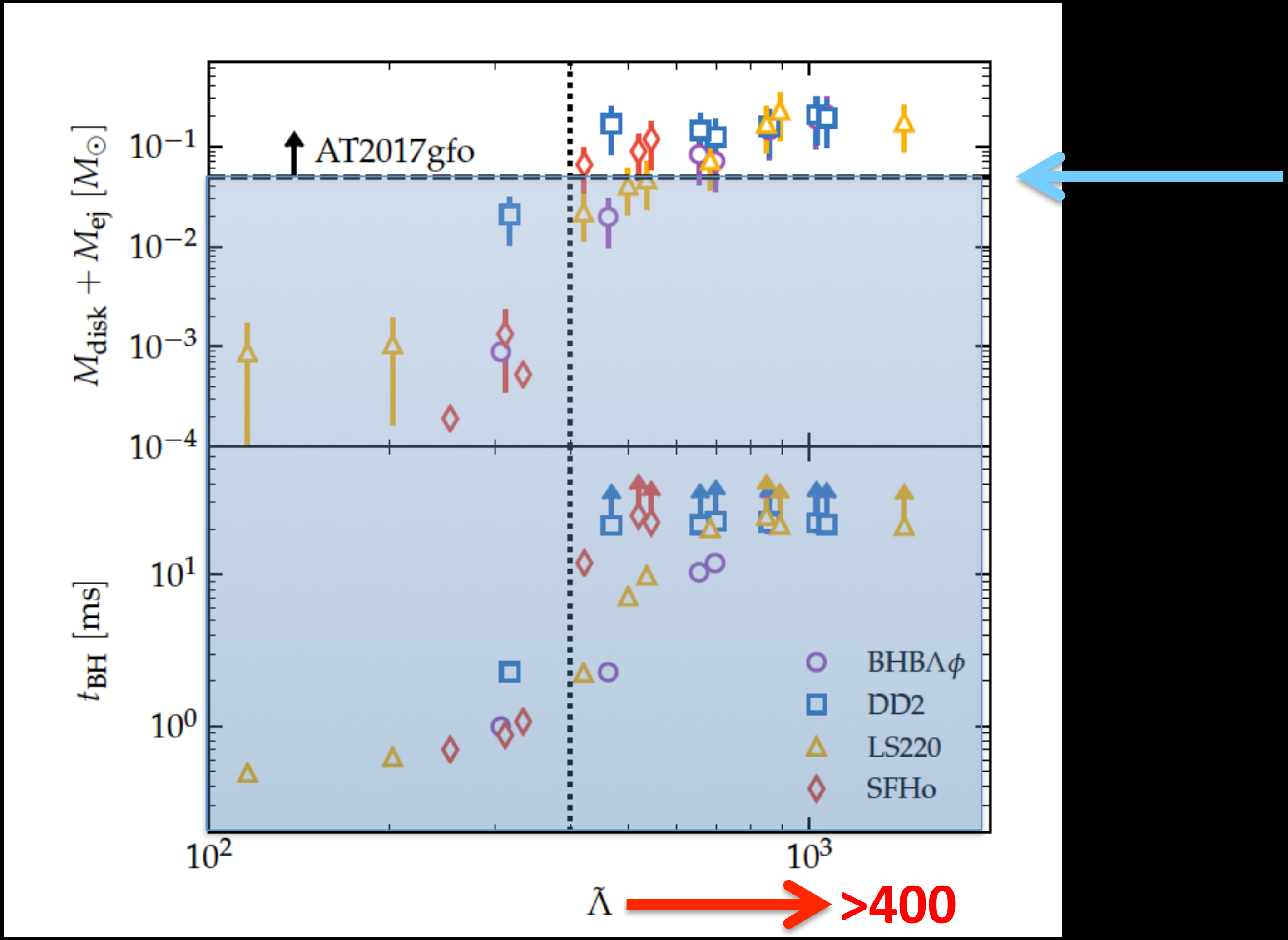

Radice, Perego, Zappa, Bernuzzi 2018

Multimessenger constraints on nuclear EOS

Simulations in NR

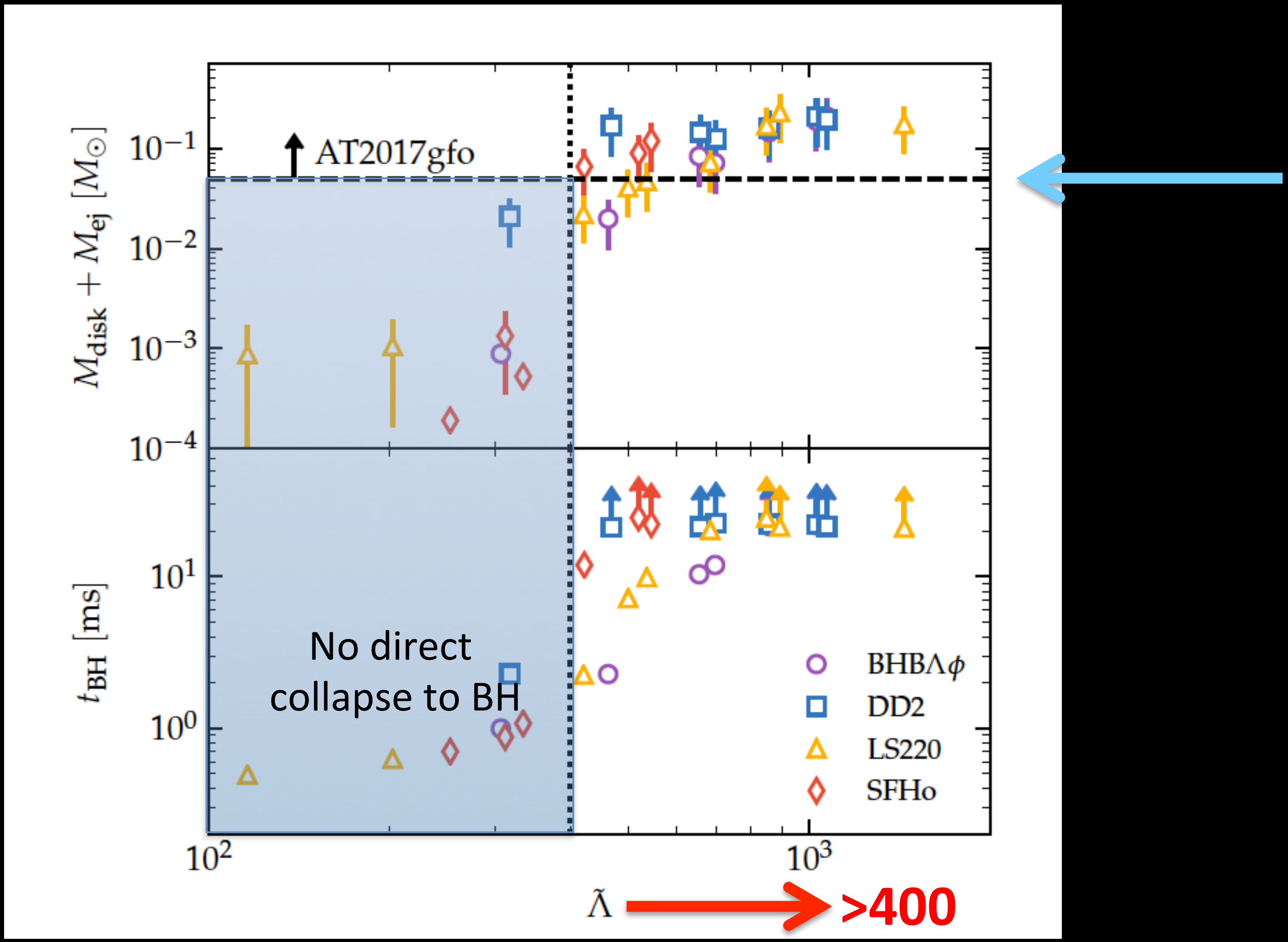

Radice, Perego, Zappa, Bernuzzi 2018

Multimessenger constraints on nuclear EOS

EM observations → Mej,tot > 0.05Mo suggests a lower limit Λ > 400

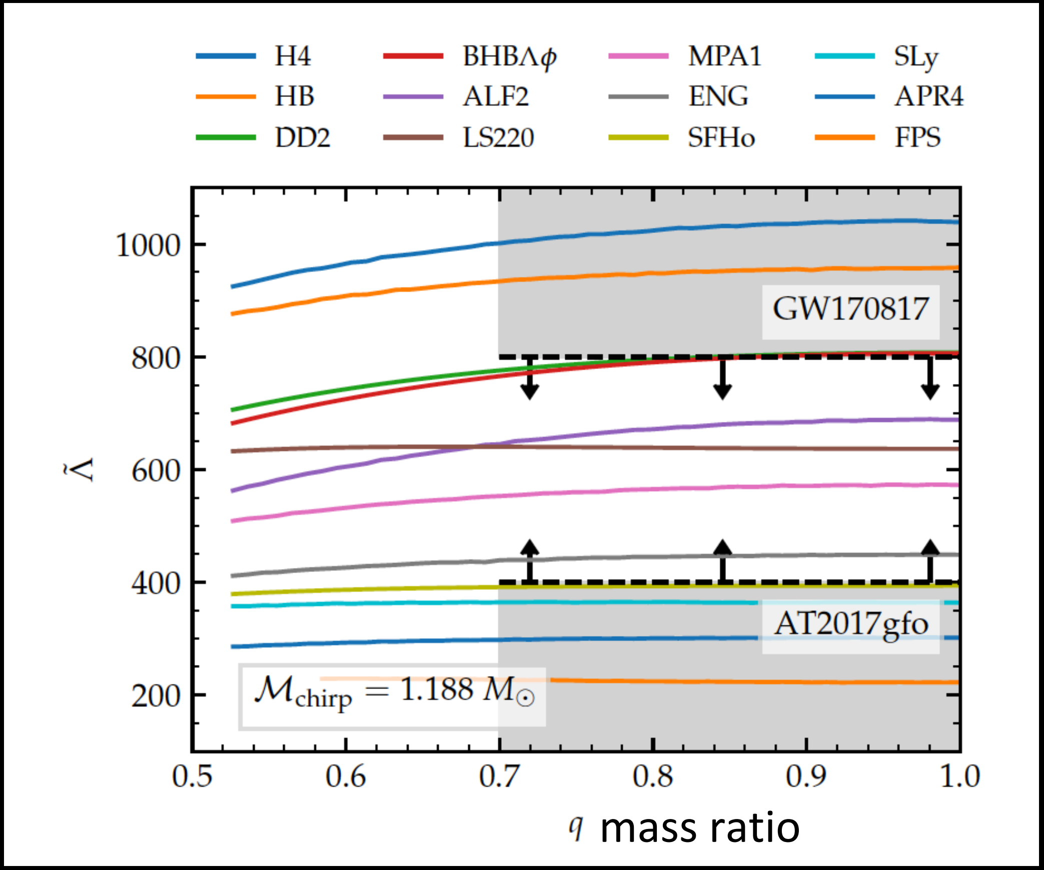

Radice, Perego, Zappa, Bernuzzi 2018

EM observations exclude very soft EOS!

EM constraints on the TYPE OF REMNANT and multi-messenger constraints on RADII and maximum MASS of (TOV) NSs

High ejecta mass
0.03 - 0.05 $M_\odot$
→ delayed/no collapse
GW Mtot < $M_{threshold}$
Bauswein+17

Blue component
ejecta 0.2-0.3 c
→ shock-heated
dynamical ejecta
Nicholl+ 17

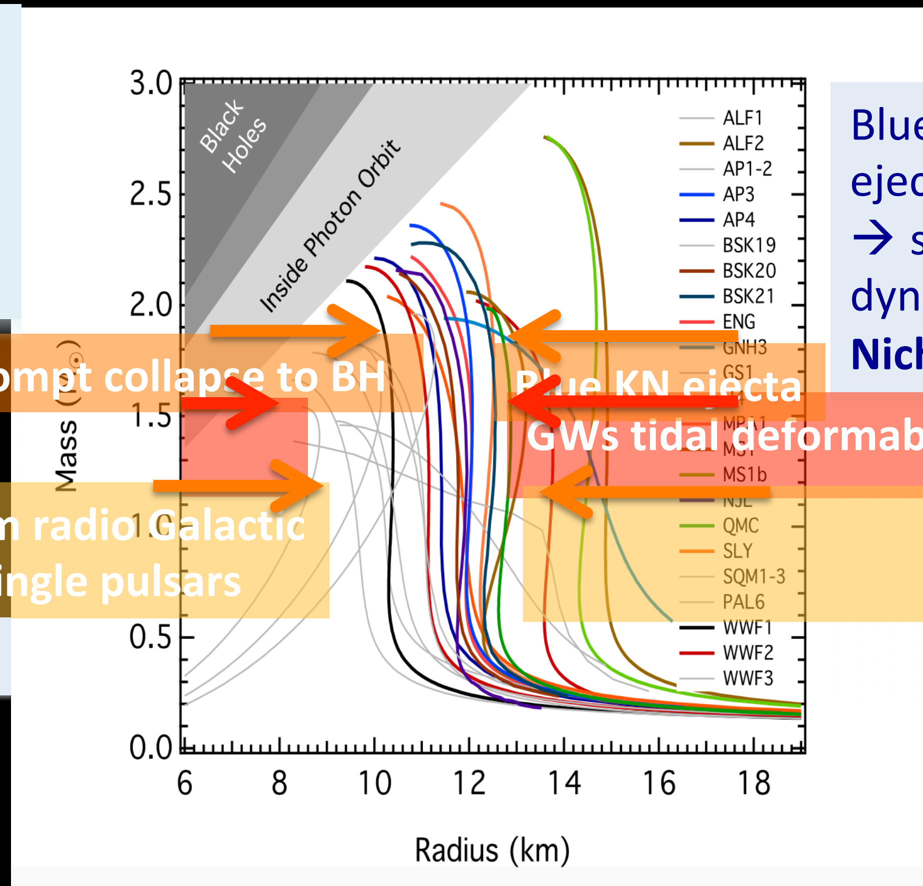

No prompt collapse to BH

Blue KN ejecta

GWs tidal deformability (LVC 18)

Mass priors from radio Galactic double NS, single pulsars

Soumi+ 18

Margalit & Metzger +17

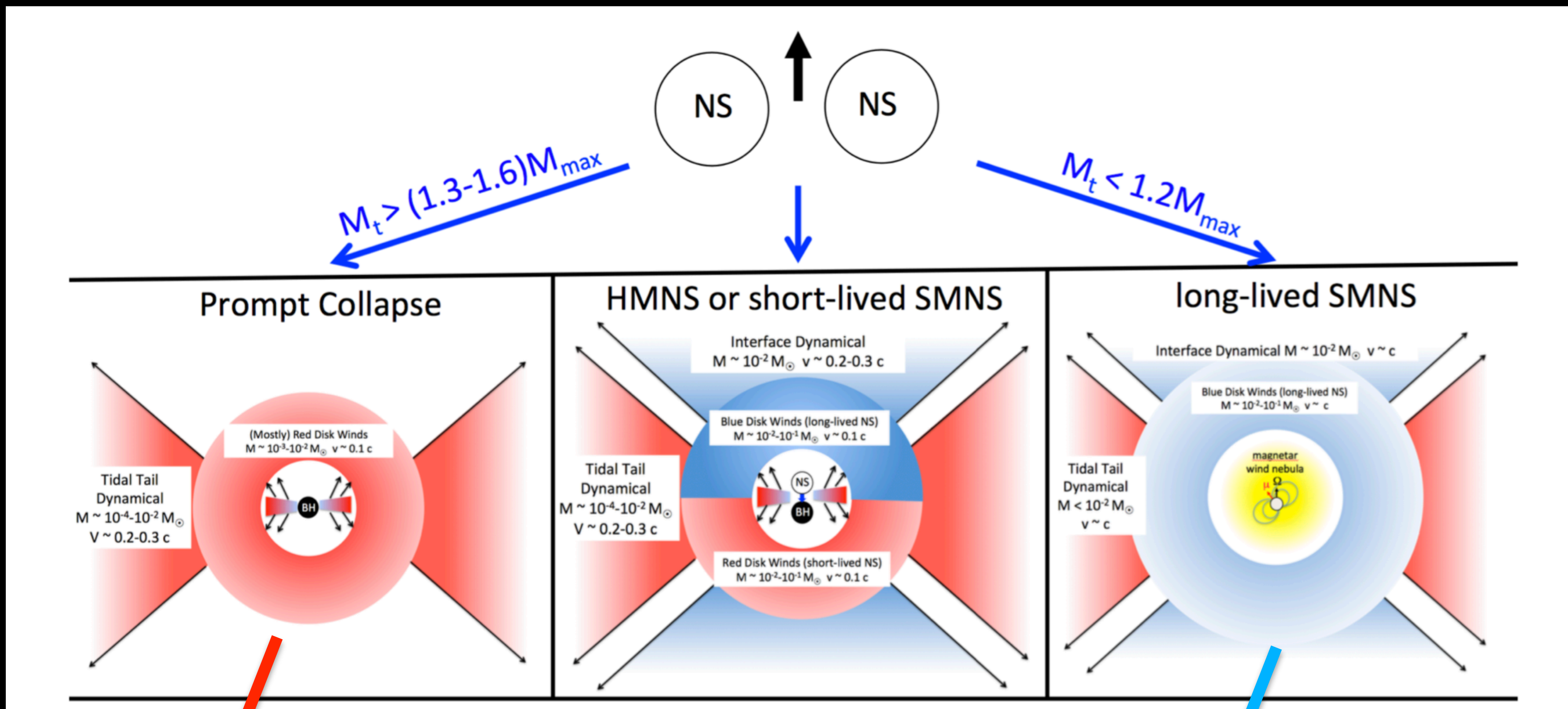

Prompt collapse to a BH:
→ polar [illegible]d ejecta and disk [illegible] negligible
→ red KN powered by the tidal ejecta

long-lived SMNS
→ imparts [illegible] large ro[illegible]onal energy to the surrou[illegible]cta, relativistic expansion [illegible]eeds to [illegible]KN ejecta or abnormally powerful GRB jet

Margalit & Metzger +17

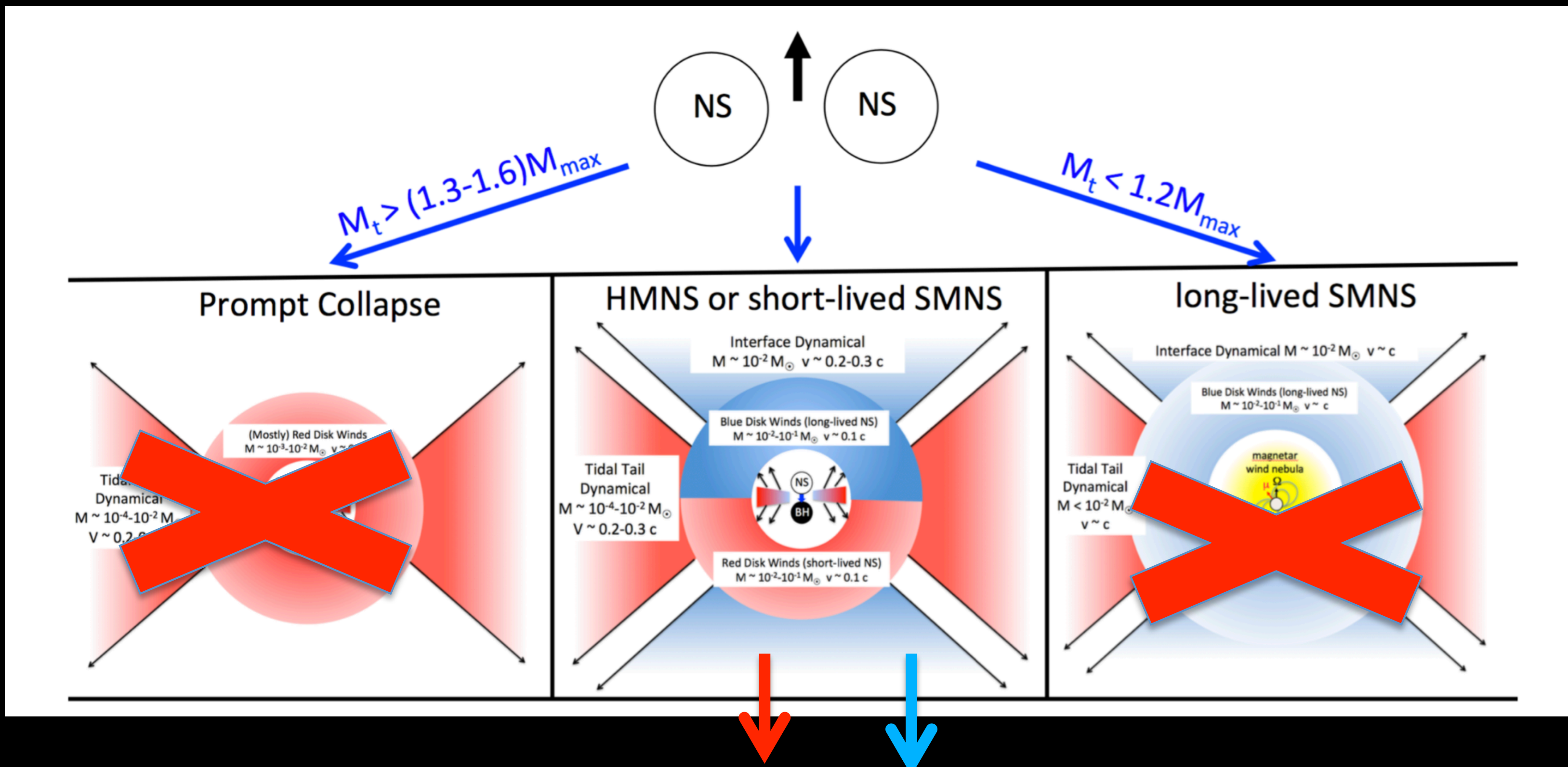

1.2Mmax < Mtot < 1.3 – 1.6 Mmax

→ HMNS or short-lived SMNS which produces both blue and red KN ejecta expanding at mildly relativistic velocities

CONSISTENT WITH OBSERVATIONS OF GW170817

EM constraints on the TYPE OF REMNANT and multi-messenger constraints on RADII and maximum MASS of (TOV) NSs

No extended high-energy emission, moderate kinetic energy for kilonova and off-axis jet, GW mass of the binary
Margalit & Metzger +17

Blue ejecta
Rezzolla+18

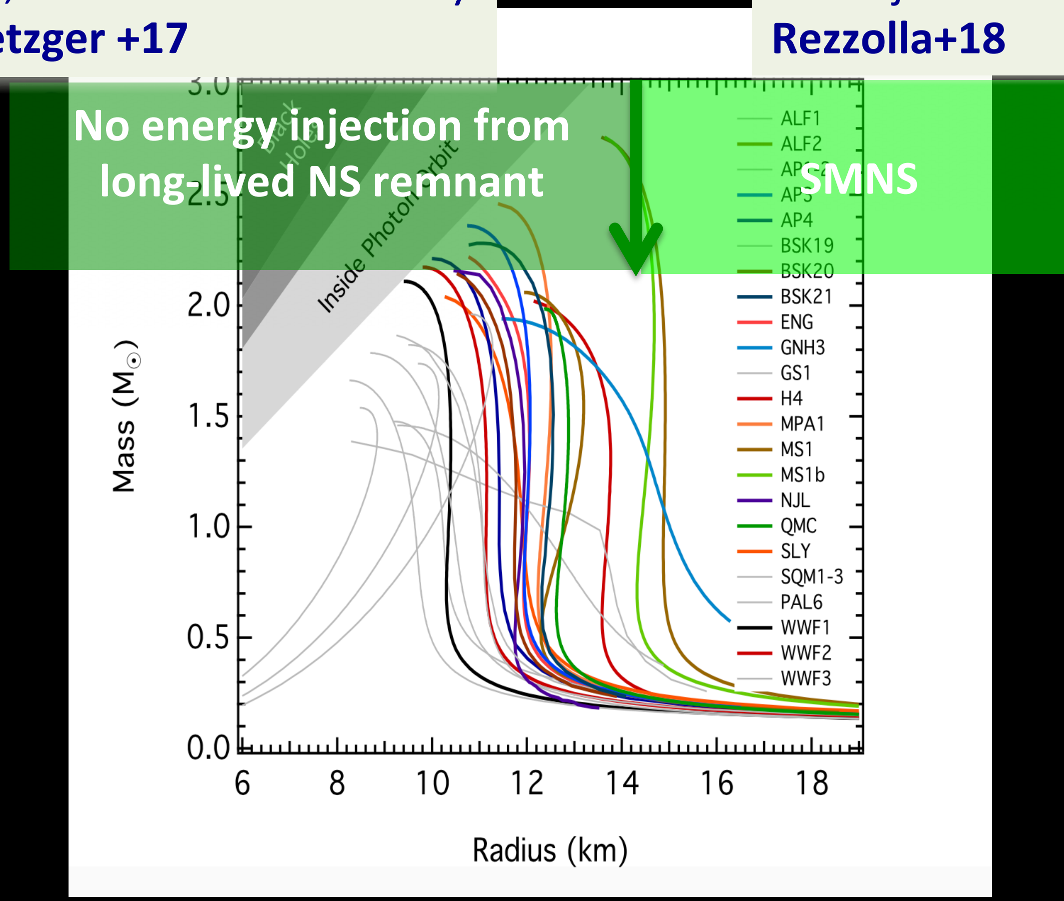

EM constraints on the TYPE OF REMNANT and multi-messenger constraints on RADII and maximum MASS of (TOV) NSs

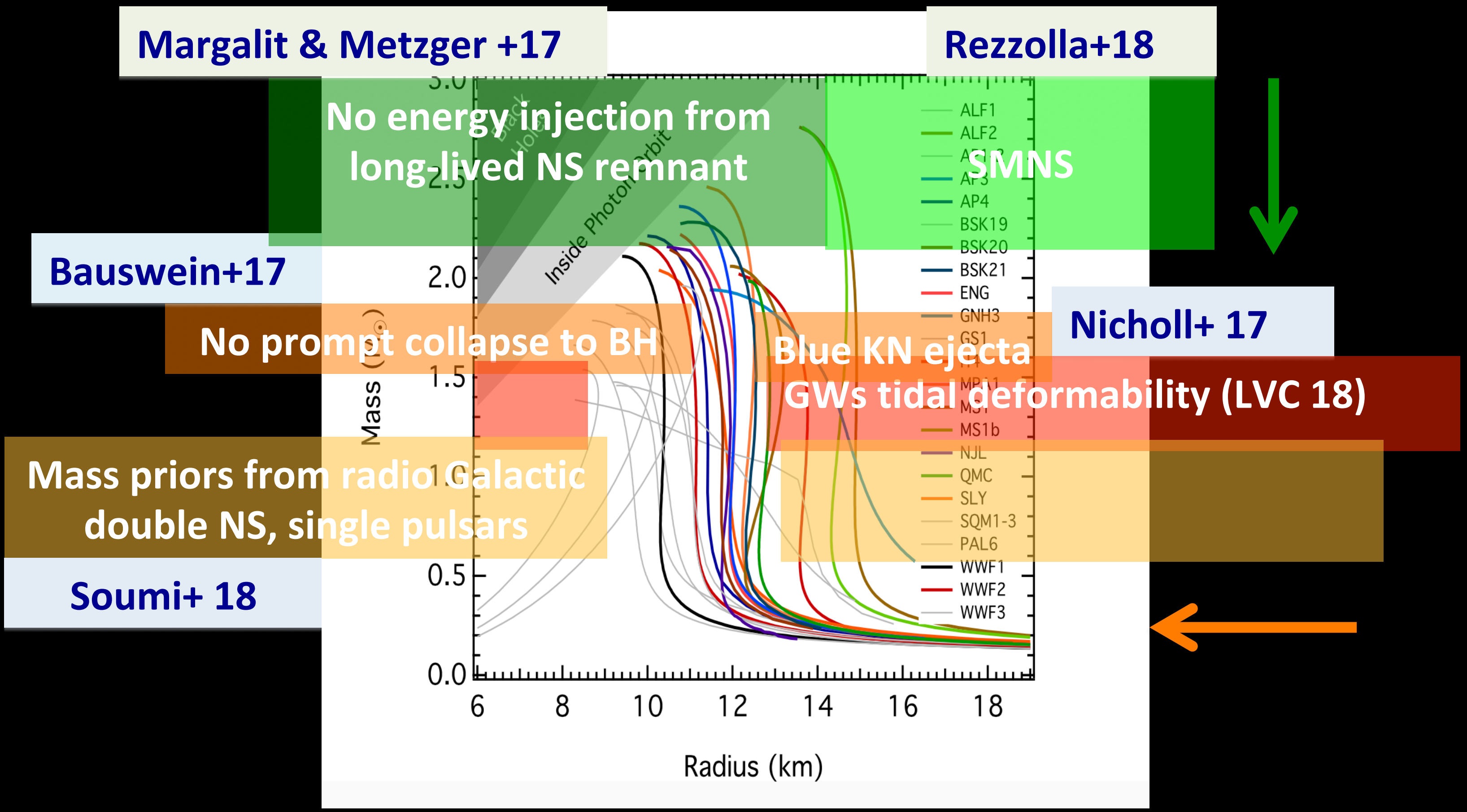

NEUTRINO SEARCHES WITH ANTARES, ICECUBE AND PIERRE AUGER OBSERVATORY

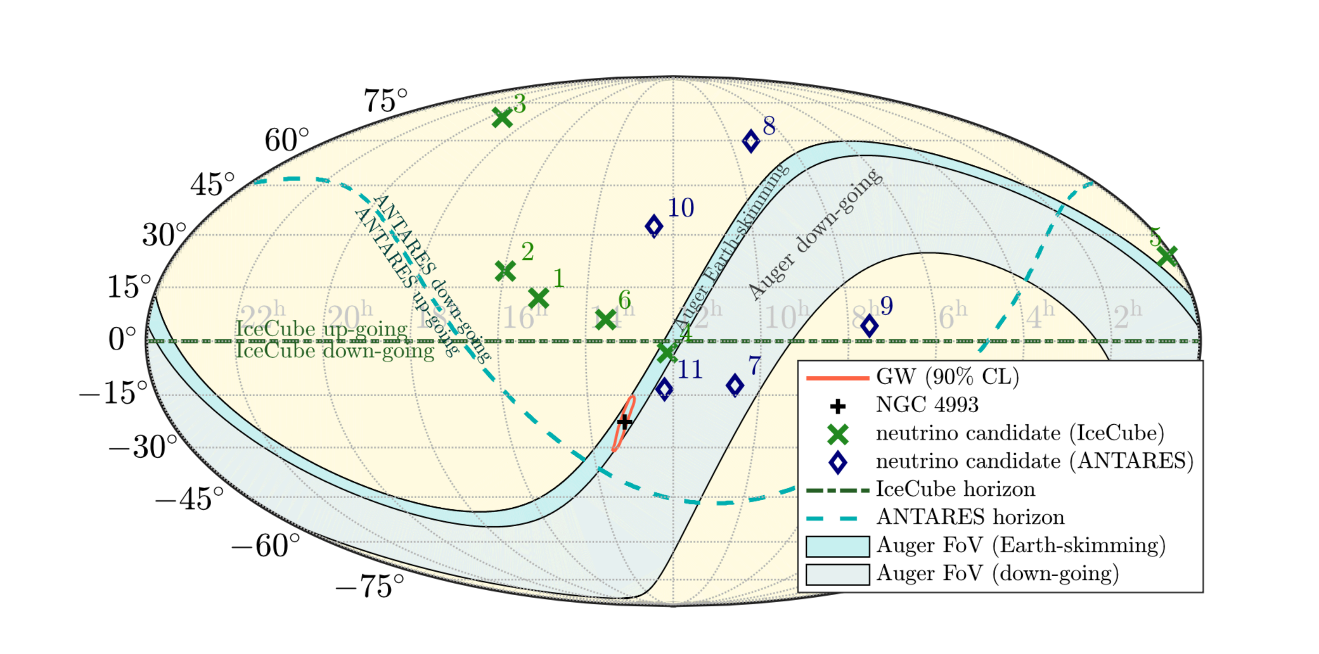

- No neutrinos directionally coincident with the source were detected within ±500 s around the merger time
- No HEN emission in the direction of the source within the 14-day period following the merger

ANTARES+IceCuce+Auger+LVC 2017, ApJ

NEUTRINO SEARCHES WITH ANTARES, ICECUBE AND PIERRE AUGER OBSERVATORY

Non-detection consistent with model predictions of short GRBs observed at a large off-axis angle

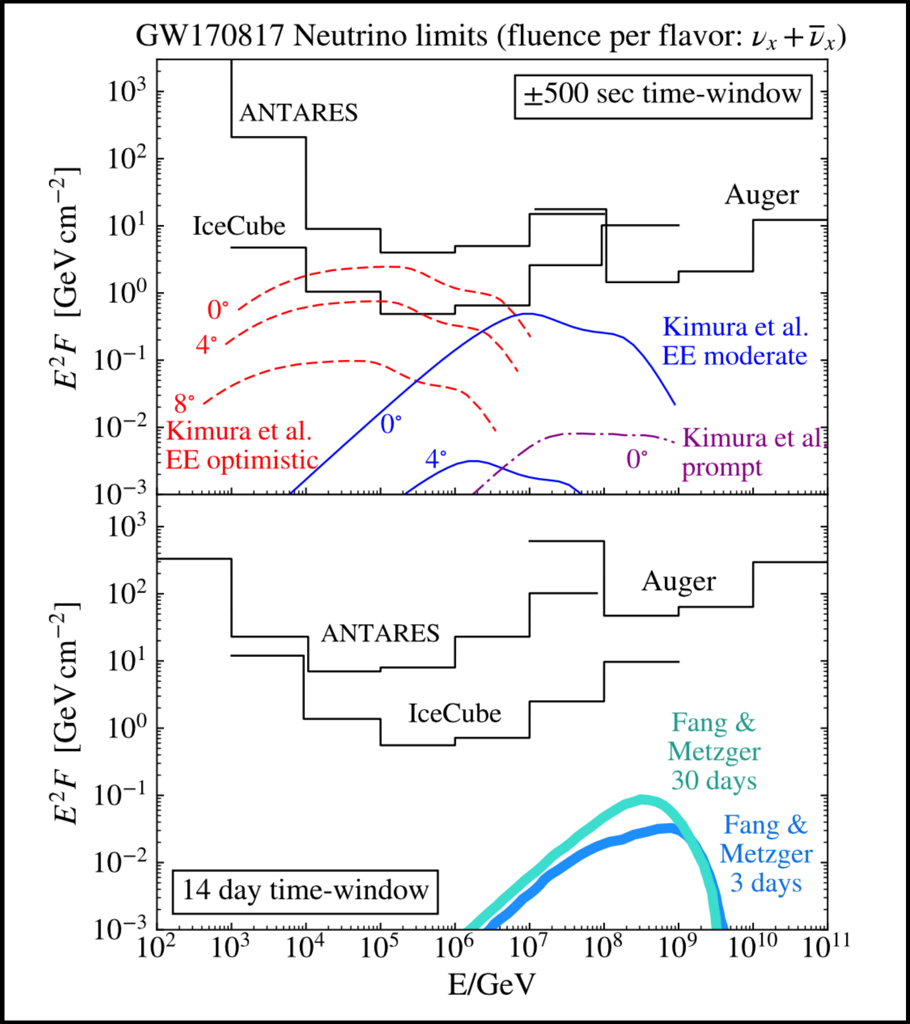

ANTARES+IceCuce+Auger+LVC 2017, ApJ

NS-NS RATE vs short GRB

- Range: the volume- and orientation-averaged distance at which a compact binary coalescence gives a matched filter SNR of 8 in a single detector;

- Distance for sGRB: distance at which an optimally (face-on → orbital plane perpendicular to the line of sight): range x 1.5

Mass: NS = 1.4 Mo

Ranges of Advanced detector in design-sensitivity
197 Mpc for NS-NS

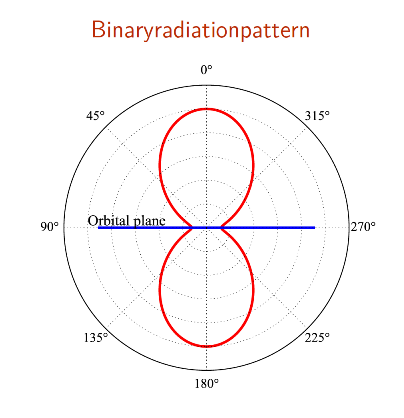

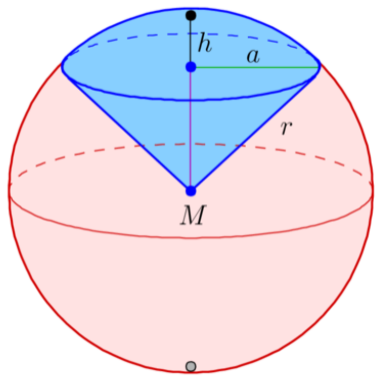

Spherical sector

$$V = \frac{2\pi r^2 h}{3} = \frac{2\pi r^3}{3}(1 - \cos\varphi)$$

half cone angle

Beaming factor

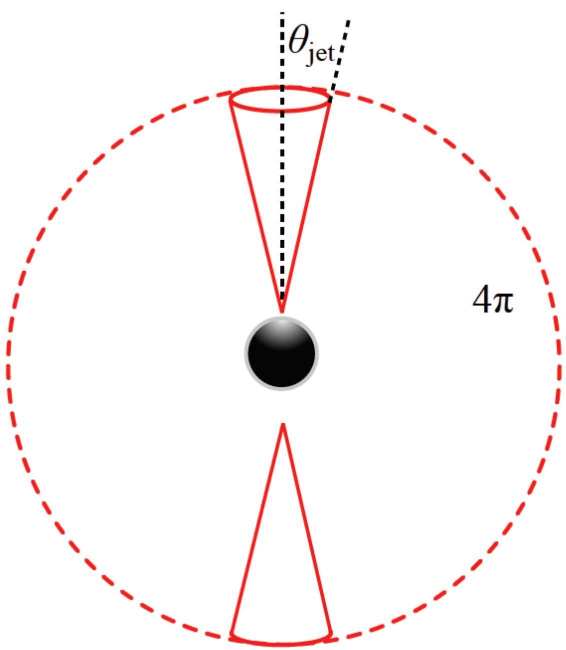

$$f_{\rm b} = \frac{2 \times 2\pi\,(1 - \cos\theta_{\rm jet})}{4\pi} = 1 - \cos\theta_{\rm jet}$$

$\theta_{\rm jet}$= jet half-opening angle

Assuming NS-NS progenitor of short GRB:

$R_{NS\text{-}NS} = R_{GRB}/(1-\cos(\theta jet))$

If not all the NS-NS produce a GRB:

$R_{NS\text{-}NS} > R_{GRB}/(1-\cos(\theta jet))$

Beaming factor

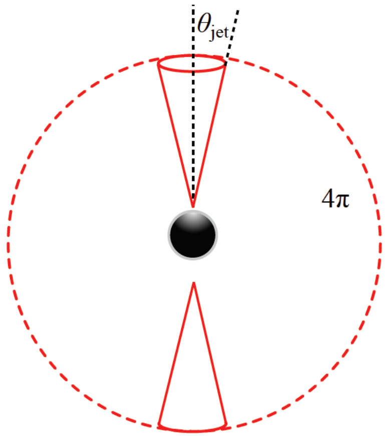

$$f_b = \frac{2 \times 2\pi\,(1-\cos\theta_{\rm jet})}{4\pi} = 1-\cos\theta_{\rm jet}$$

$\theta_{\rm jet}$= jet half-opening angle

The energy luminosity of GRB is typically given as Isotropic-equivalent: the energy release assuming that the GRB radiates isotropically

$$E = E_{\rm iso} f_{\rm b}$$

$$L = L_{\rm iso} f_{\rm b},$$

BEAMING CORRECTION FOR ENERGY AND LUMINOSITY FROM ISOTROPIC VALUE

where

$$f_{\rm b} = 1 - \cos\theta_{\rm j} \simeq \theta_{\rm j}^2/2.$$

BEFORE GW170817…..

Short GRB rate → GW/sGRB detections by aLIGO/Virgo

R_{GRB} = 0.4-4 Gpc^{-3} yr^{-1} (e.g. Ghirlanda et al 2016, Wanderman & Piran 2015)

→ **$R_{GRB/GW}$ (300* Mpc) = 0.04-0.4 yr^{-1}** *in full sensitivity (range 200 Mpc)*

(*Distance range for NS-NS times 1.5 for face-on systems)

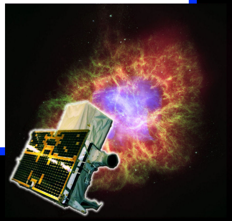

sGRB rate → NS-NS aLIGO/Virgo detection rate

Assuming NS-NS progenitor of short GRB:

$$R_{NS\text{-}NS}=R_{GRB}/(1-\cos(\theta j))$$

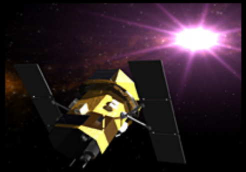

For θj = 10 deg → **$R_{NS\text{-}NS}$ (200* Mpc) = 0.9-10 yr^{-1}**

Jet half-opening angle measure

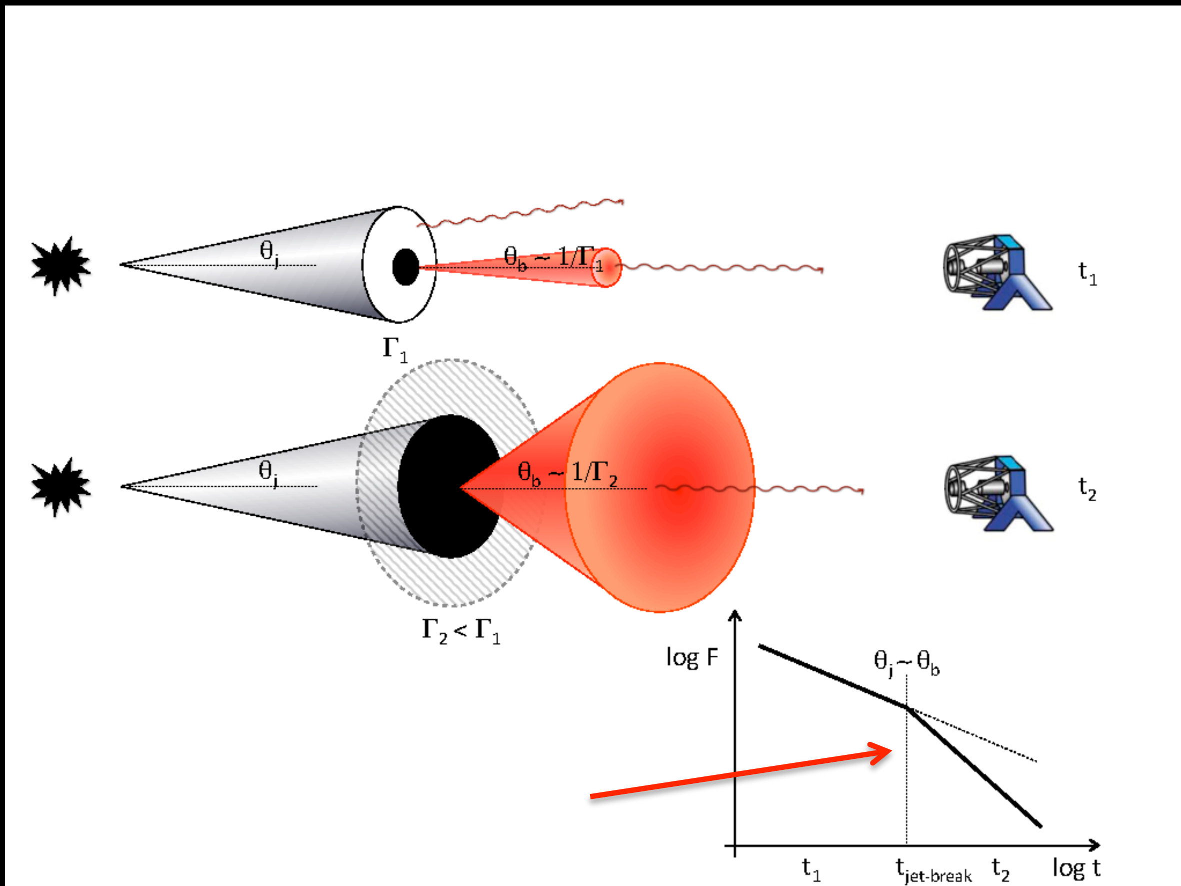

- relativistic opening angle $\theta_b = 1/\Gamma$ (within which ejecta radiates) increases due to the ejecta deceleration
- Jet break when θ_b equals the jet cone aperture θjet

Flux reduction of $\theta_{jet}{}^2/(1/\Gamma)^2 = \theta_{jet}{}^2\,\Gamma^2$

Mostly due to edge (geometric) effect: the $1/\Gamma$ is no longer filled by the emission beyond the jet break time (when $1/\Gamma > \theta_{jet}$)

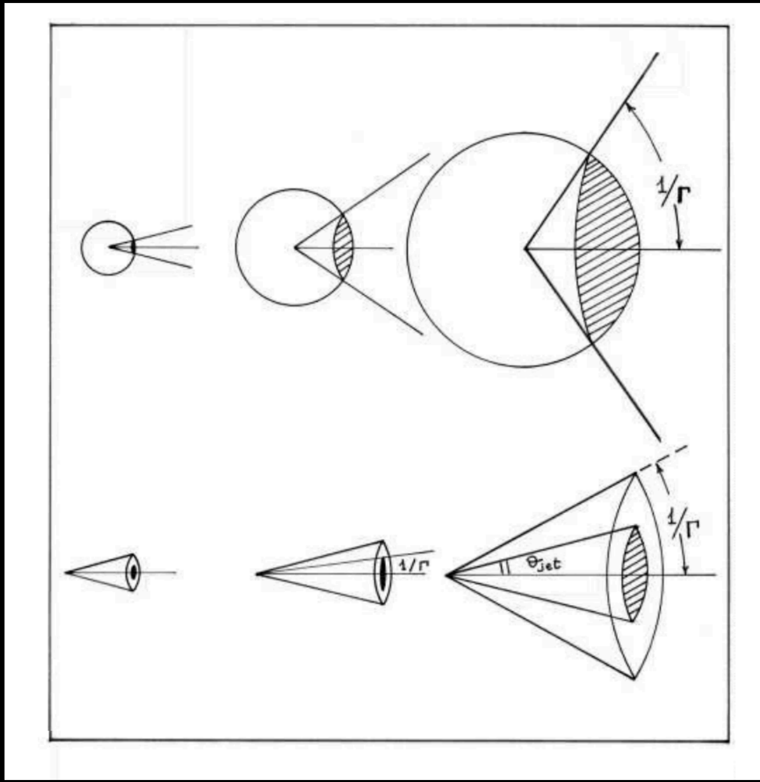

Ghisellini 2001

- During the initial phases of the afterglow, the bulk Lorentz factor is large → the observer sees only the fraction of the emitting area inside a cone with aperture angle ~ 1/Γ.

NO DIFFERENCE BETWEEN A SPHERE AND A JET!

SPHERICAL CASE the emitting area increase because the radius of the sphere increases and because Γ decreases, allowing more surface to be within the 1/Γ cone

COLLIMATED JET once 1/Γ becomes comparable to the jet opening angle θ, the observed surface increases only because the distance to the jet apex increases.

The light curve predicted in the two cases is the same at early times, but in the jet case there will be a break at the time (when 1/Γ ~ θ), after which the light curve decreases more rapidly than in the spherical case

Jet half-opening angle measure

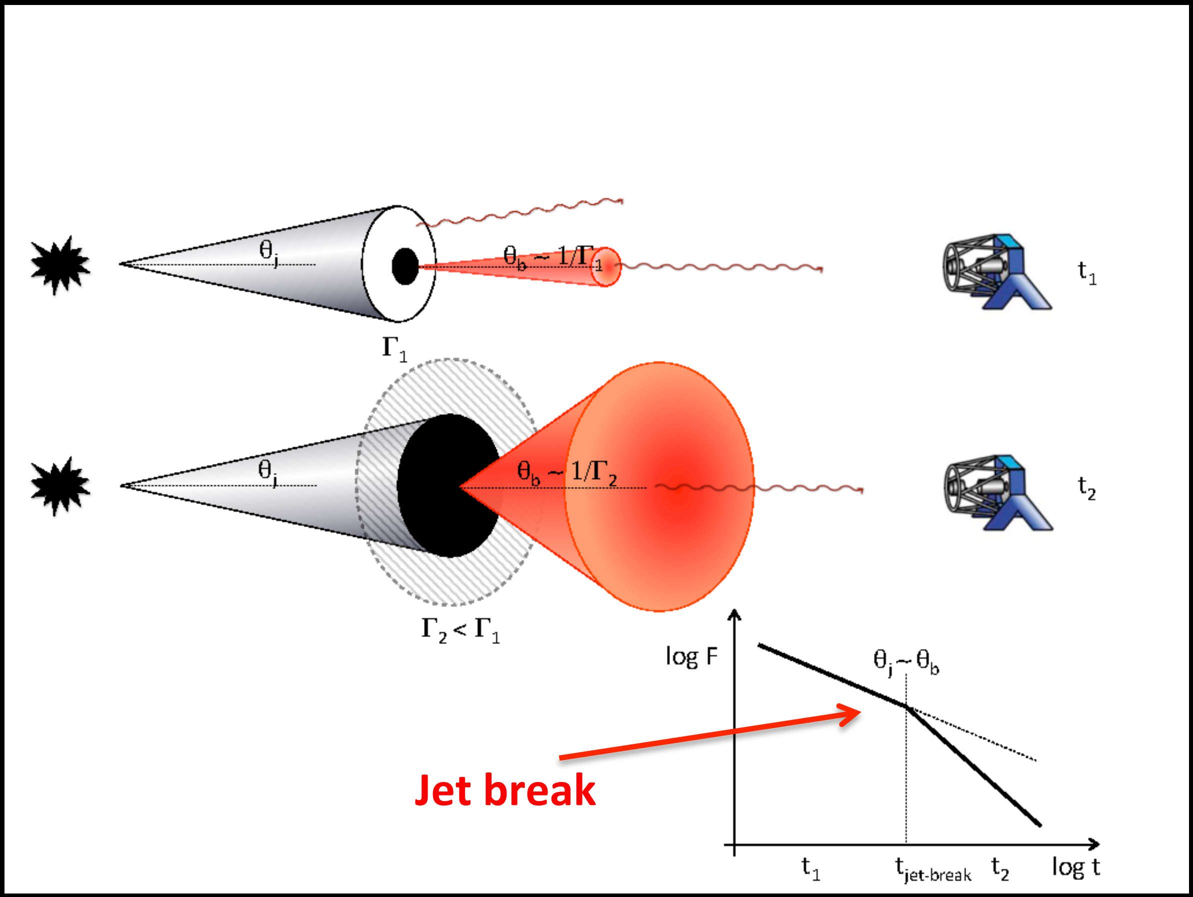

- relativistic opening angle $\theta_b = 1/\Gamma$ (within which ejecta radiates) increases due to the ejecta deceleration
- Jet break when θ_b equals the jet cone aperture θjet

$$1/\Gamma(t_{\text{jet-break}}) = \theta_j = 0.13\left(\frac{t_{j,d}}{1+z}\right)^{3/8}\left(\frac{n_0}{E_{52}}\right)^{1/8}$$

Sari, Piran and Halpern 1999

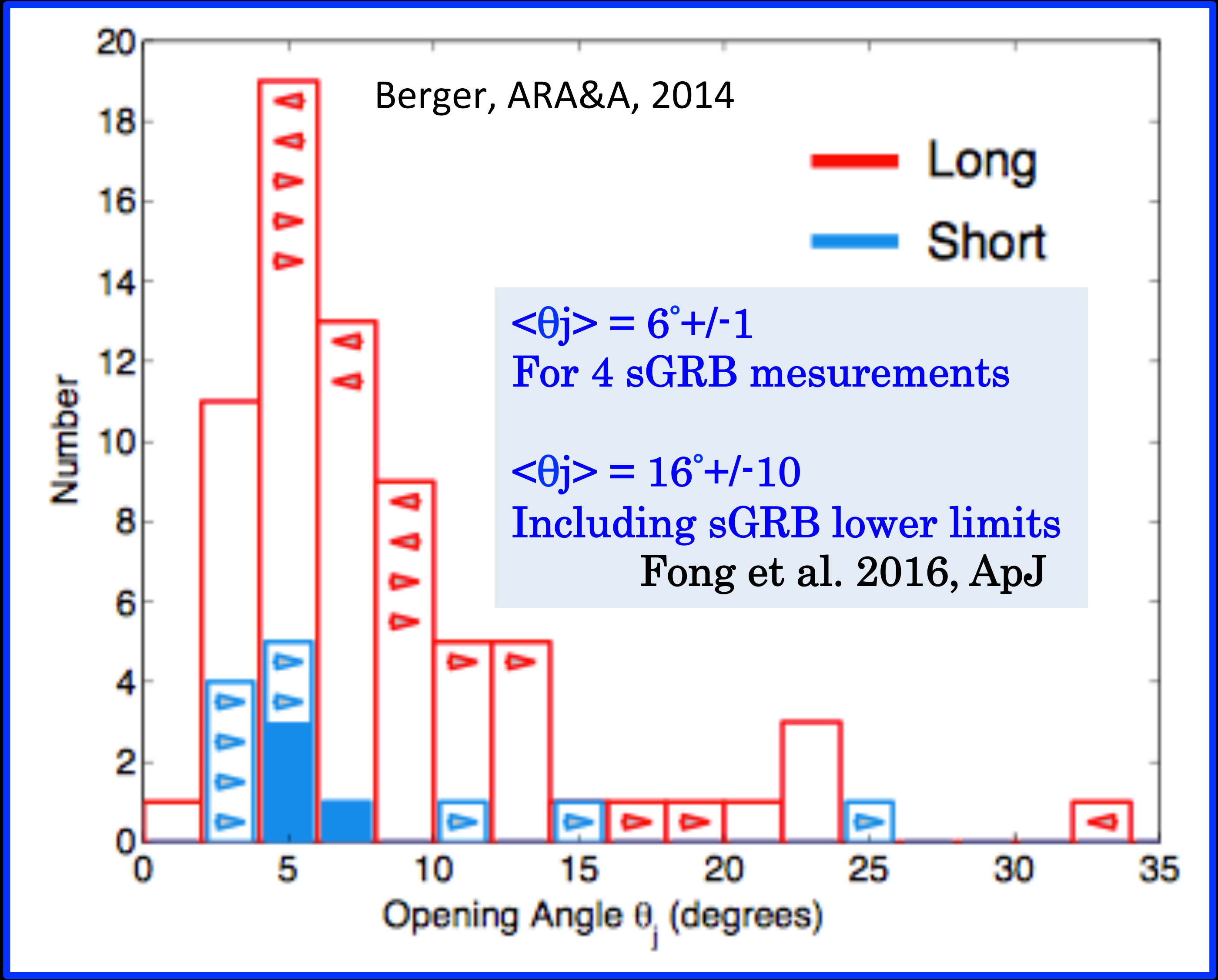

Berger, ARA&A, 2014
Long
Short
<θj> = 6°+/-1
For 4 sGRB mesurements
<θj> = 16°+/-10
Including sGRB lower limits
Fong et al. 2016, ApJ
Number
Opening Angle θj (degrees)
0
5
10
15
20
25
30
35
0
2
4
6
8
10
12
14
16
18
20

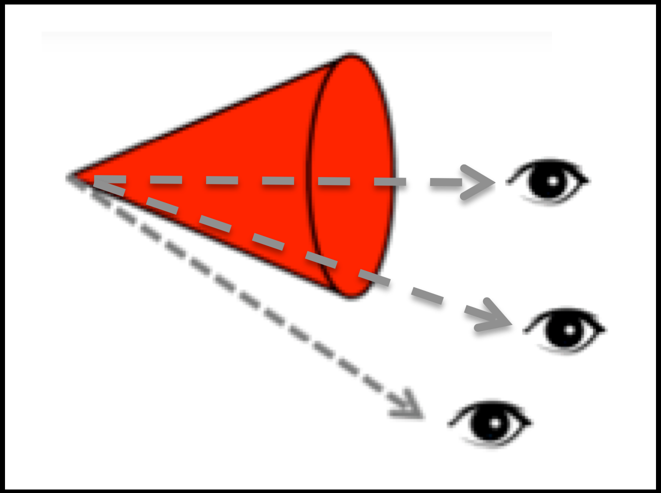

GW170817/GRB170817A

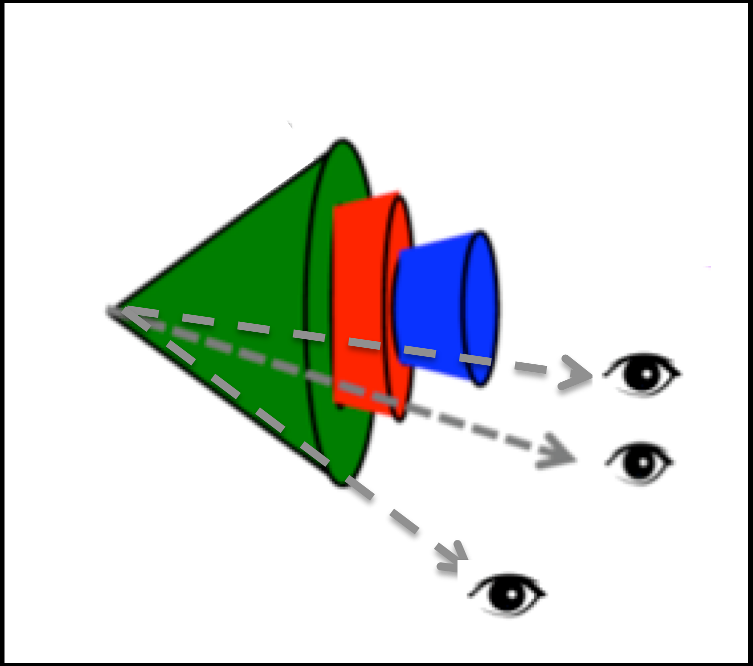

If such a jet observed on-axis → isotropic equivalent luminosity ≥ 10^{51} erg s^{-1}

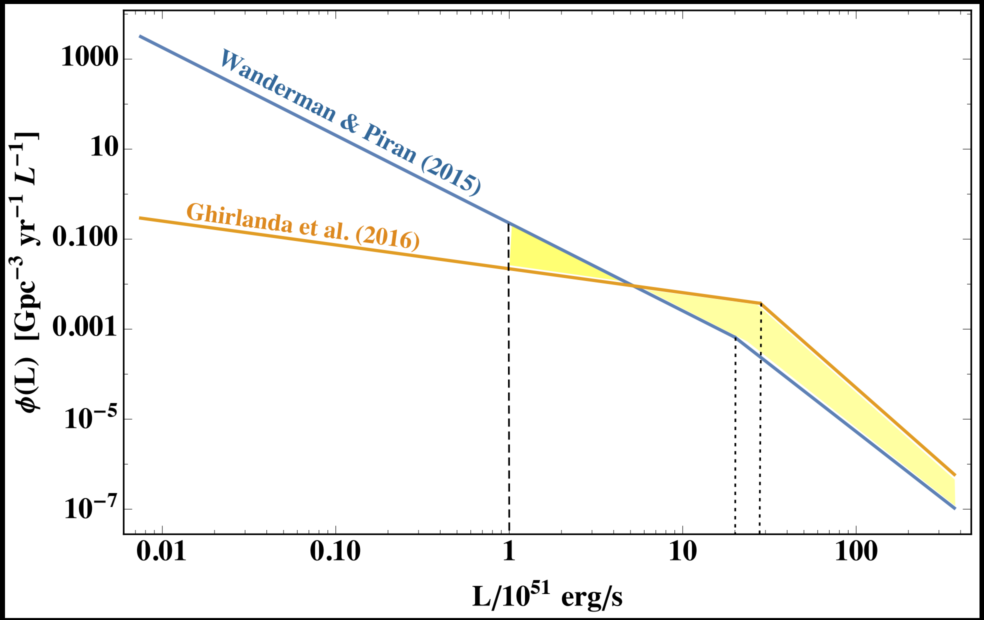

Luminosity function (FdL)

Rate per volume for sGRB with L > L_min:

$$\int_{L\min}^{\infty} \phi(L)\, dL$$

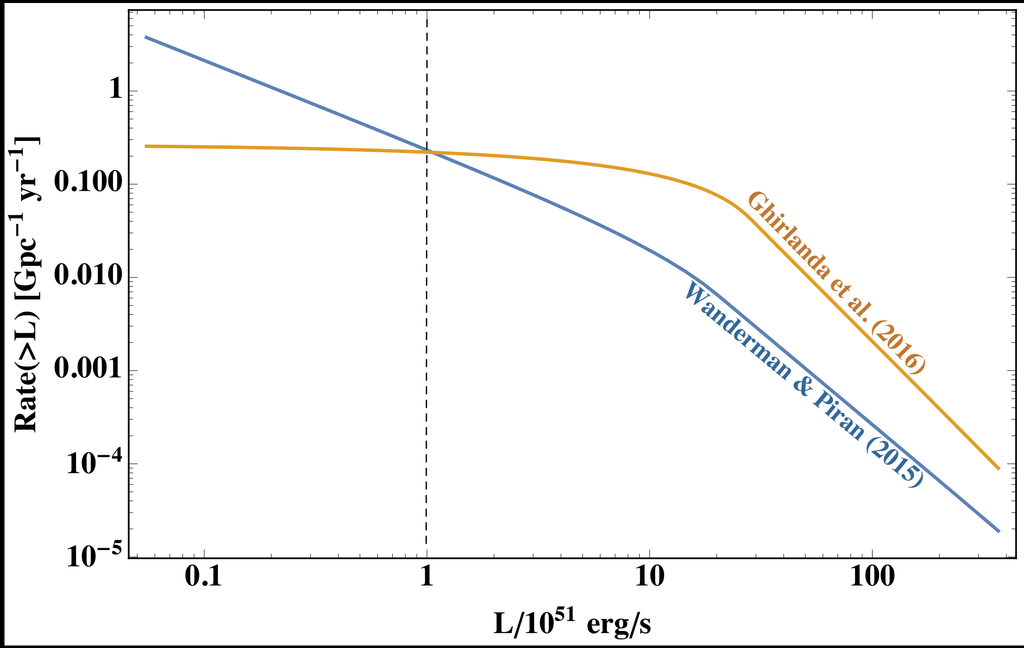

GW170817/GRB170817A

FERMI/GBM RATE for event like GRB170817A
Liso~10^{47} erg s^{-1}

$$N_{sGRB}(GBM) = \frac{\Omega_{GBM} T_{GBM}}{4\pi} \rho_{0.SGRB} V_{\max}$$

$$\Omega_{GBM} \approx 4\pi$$

$$T_{GBM} = 9\text{yr} * 0.5 \text{ (duty cycle)}$$

$$V_{\max} = 65 \ Mpc$$

$$\Rightarrow 190^{+440}_{-160} \text{Gpc}^{-3} \text{ yr}^{-1}$$

Zhang, B.B et al. 2018, Nature Com
Ghirlanda et al. 2018, Science 2019

See also Della Valle et al. 2018

$$352^{+810}_{-281} \text{ Gpc}^{-3} \text{ yr}^{-1}$$

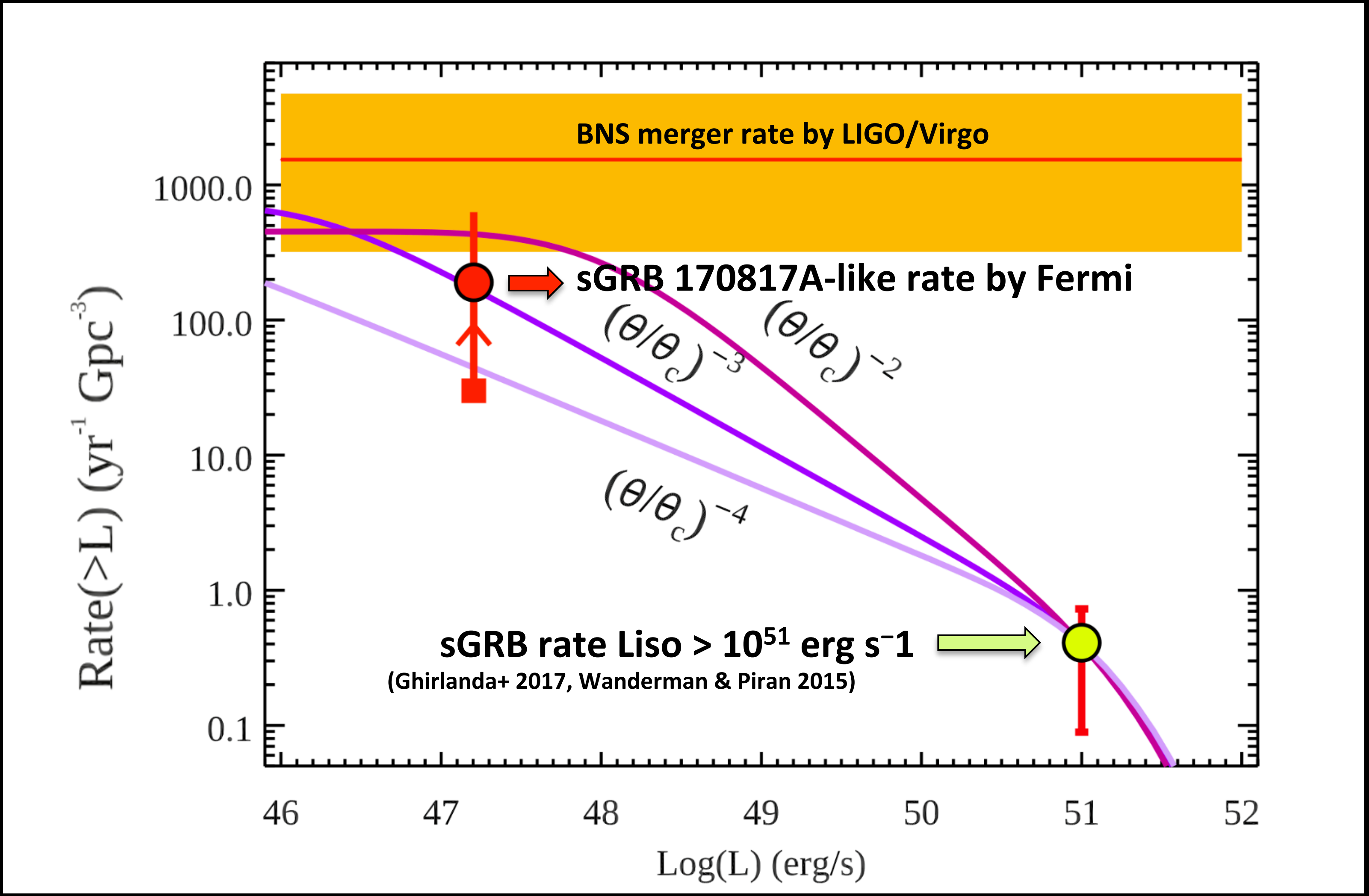

Ghirlanda et al. 2019, Science 2019

Assuming all sGRB are similar to GW170817, and sGRB with Liso > 10^{51} erg s^{-1} produced by jets whose core points to us:
→ number of lower luminosity events increases according to the jet structure

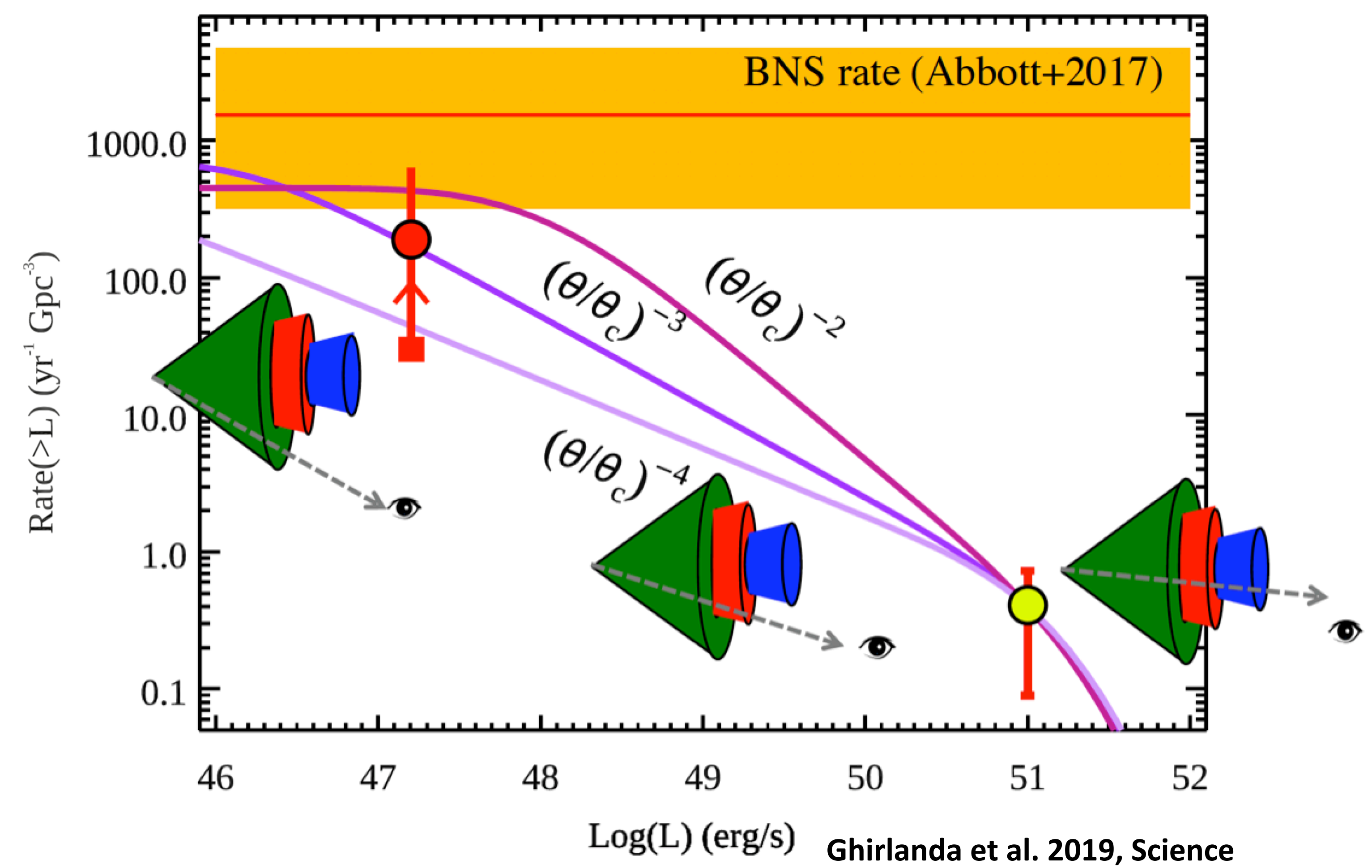

Ghirlanda et al. 2019, Science

The rate of GRBs with luminosity as low as GRB 170817A is consistent with the luminosity function of structured jets!

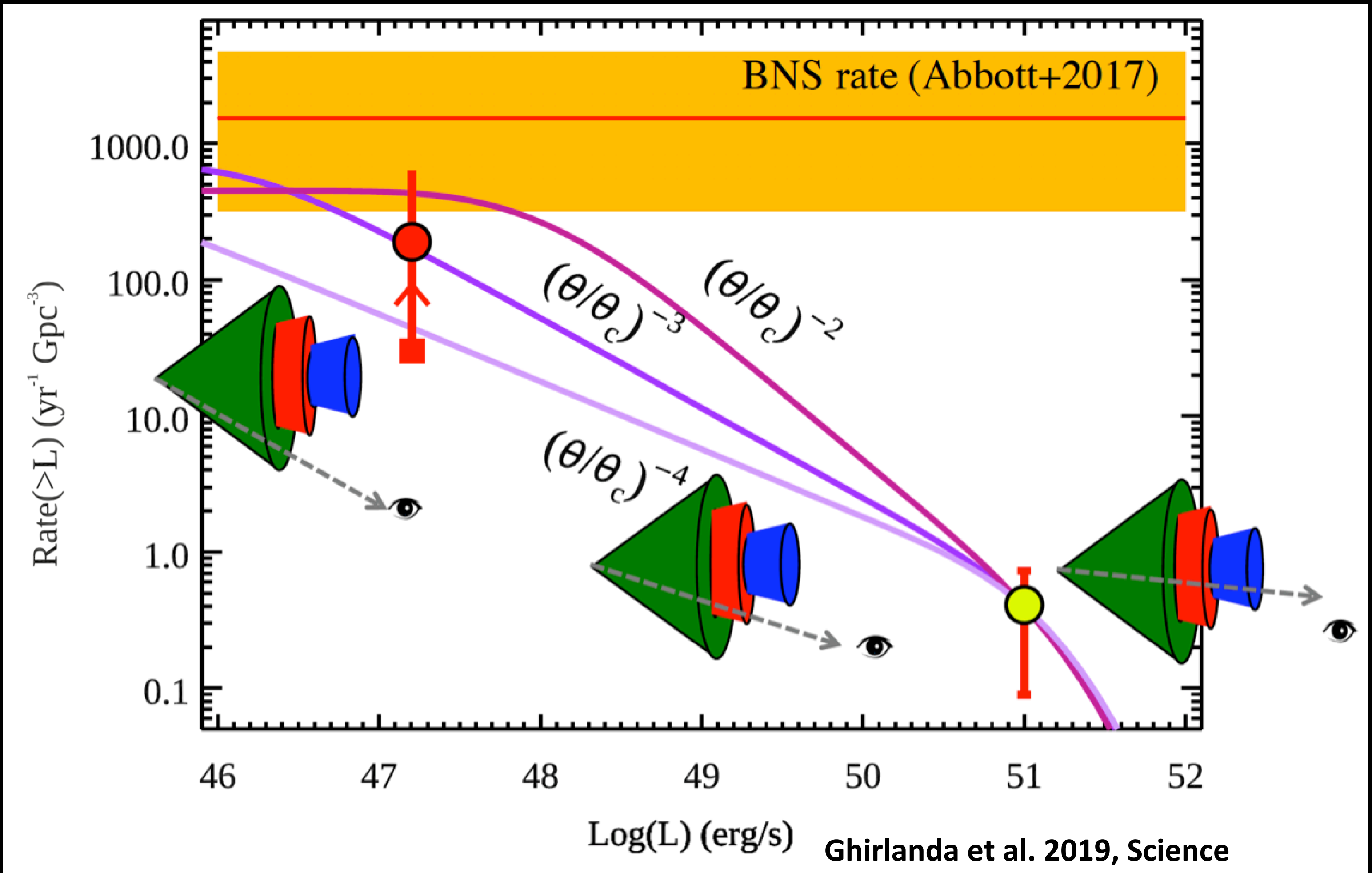

Comparison with LIGO and Virgo BNS rate → at least 10% of NS- NS mergers launch a jet which successfully breaks out of the merger ejecta